J Comput Aided Mol Des (2012) 26:1369–1388
DOI 10.1007/s10822-012-9621-7

A novel view of modelling interactions between synthetic and biological polymers via docking

Vladimir B. Tsvetkov · Alexander V. Serbin

Received: 16 August 2012 / Accepted: 27 November 2012 / Published online: 13 December 2012

Abstract Multipoint interactions between synthetic and natural polymers provide a promising platform for many topical applications, including therapeutic blockage of virus-specific targets. Docking may become a useful tool for modelling of such interactions. However, the rigid docking cannot be correctly applied to synthetic polymers with flexible chains. The application of flexible docking to these polymers as whole macromolecule ligands is also limited by too many possible conformations. We propose to solve this problem via stepwise flexible docking. **Step 1** is docking of separate polymer components: (1) *backbone units* (**BU**), multi-repeated along the chain, and (2) *side groups* (**SG**) consisting of *functionally active elements* ($\mathbf{SG_F}$) and *bridges* ($\mathbf{SG_B}$) linking $\mathbf{SG_F}$ with **BU**. At this step, probable binding sites locations and binding energies for the components are scored. **Step 2** is docking of component-integrating models: $\mathbf{[BU]}_m$, $\mathbf{SG = SG_F–SG_B}$, **BU–SG**, **BU–BU(SG)–BU**, **BU(SG)–**$\mathbf{[BU]}_m$**–BU(SG)**, and $\mathbf{[BU}_{var}\mathbf{(SG}_{var}\mathbf{)]}_m$. Every modelling level yields new information, including how the linkage of various components influences on the ligand—target contacts positioning, orientation, and binding energy in step-by-step approximation to polymeric ligand motifs. **Step 3** extrapolates the docking results to real-scale macromolecules. This approach has been demonstrated by studying the interactions between hetero-SG modified anionic polymers and the N-heptad repeat region tri-helix core of the human immunodeficiency virus type 1 (**HIV-1**) envelope glycoprotein gp41, the key mediator of HIV-1 fusion during virus entry. The docking results are compared to real polymeric compounds, acting as HIV-1 entry inhibitors in vitro. This study clarifies the optimal macromolecular design for the viral fusion inhibition and drug resistance prevention.

Keywords Docking · Polymer–polymer interaction · Drug design · Maleic acid copolymer · HIV fusion inhibitor · Glycoprotein gp41

Introduction

Molecular docking is widely used in computational modelling to explore the preferred sites, orientation, and energy of binding between two molecular partners [1, 2]. As a rule, one of them is a biologically relevant macromolecule (e.g., a protein or nucleic acid), defined as a target, and the other, regarded as a ligand docked to the target, is usually a low-molecular-mass compound [3]. Studies on such ligands are in line with the interests of traditional medical science regarding small molecular drugs [3, 4], but development of the most promising therapeutics depends on novel drug design strategies based on synthetic (or hybrid) polymers [5–7]. This requirement implies an increasing necessity of modelling the behaviour of such high molecular ligands.

V. B. Tsvetkov
Orekhovich Institute of Biomedical Chemistry, RAMS, Pogodinskaya St. 10/8, 119121 Moscow, Russia

V. B. Tsvetkov · A. V. Serbin
Topchiev Institute of Petrochemical Synthesis, RAS, Leninsky Prospect 29, 119991 Moscow, Russia

V. B. Tsvetkov
Computing Analysis Center, Health RDF, Boulevard Adm. Ushakova 14-209, 117042 Moscow, Russia
e-mail: v.b.tsvetkov@gmail.com

A. V. Serbin (✉)
Biomodulators and Drugs RC, Health RDF, Boulevard Adm. Ushakova 14-209, 117042 Moscow, Russia
e-mail: heal@aha.ru; serbin@ips.ac.ru

The current level of docking techniques does not allow modelling of the interactions of synthetic polymers with natural macromolecules. Most importantly, an entire synthetic polymer molecule (unlike a small molecule) cannot be docked directly as a single ligand when simulating a flexible polymer chain. The applicability of *flexible docking* [8, 9] in this case is limited by the high conformational capacity of polymers (up to $10^{(2-3)N}$ for *N*-mer chains[1]), full calculation of which requires immense computational time and power. *Rigid docking*, usually applied in modelling polymer–polymer (e.g., protein–protein) interactions [1], could be more suitable if the basic mode of ligand–target spatial assembly is known a priori or is predictable. In practice, however, we deal with indefinite ligand conformations, and therefore extensive diversity of alternative polymer–target interactions. Under such conditions, application of the rigid docking approach makes it necessary to scan the entire ensemble of all possible conformations. In principle, this method could be executable, but it is far beyond the capacity of current computational experiments (at the currently accessible computing power).

In this paper, we propose an algorithm for overcoming these problems and demonstrate its applicability by studying the docking of the *side-group variable derivatives of synthetic maleic acid copolymers* as macro-ligands to the *protein-type nano-mediators* of the *human immunodeficiency virus type 1* (**HIV-1**) *envelope fusion* with the cell membrane. The computational docking results (in silico) were compared with in vitro experimental data on anti-HIV activity of the same copolymers [7, 12–19]. The results were used to explain the most probable molecular mechanisms for the recorded antiviral effects. We also considered some of the fundamental differences between the low- and high-molecular-mass compounds in relation to polymer-cooperative effects (inter-polymer recognition, multipoint binding for best effectiveness and drug resistance prevention) as novel perspectives for drug design.

The modelling strategy and objects

The docking strategy proposed for polymeric macro-ligands

The general principles and procedure of the proposed molecular docking algorithm were as follows:

Step 1. Sub-structural modelling by docking not the whole macromolecule of a synthetic polymer (as a macro-ligand) but its separate components (as small molecular ligands). (1) The main polymeric chain backbone unit(s) (**BU**), multi-repeated along the chain, and (2) the side group(s)/branch(es) (**SG**), consisting of functionally active element(s) ($\mathbf{SG_F}$) and bridges ($\mathbf{SG_B}$) linking SG_F with BU. At this step, we try to identify probable binding sites and to score binding energies for all of the components.

Step 2. Integrative modelling via flexible docking of models reconstructing integration of the components into representative polymeric motifs: $[\mathbf{BU}]_m$, $\mathbf{SG_F–SG_B} = \mathbf{SG}$, **BU–SG = BU(SG)**, **BU–BU(SG)–BU**, **BU(SG)–**$[\mathbf{BU}]_{\boldsymbol{m}}$**–BU(SG)**,…, and $[\mathbf{BU}_{\boldsymbol{var}}(\mathbf{SG}_{\boldsymbol{var}})]_{\boldsymbol{m}}$. Every modelling level yields new information: how different components contribute to positioning, orientation, and binding energy as they are being linked to each other, and how this cooperation into polymeric motifs modulates interactions with the target (polymer-cooperative effects). The modelled degree of polymerisation ($\boldsymbol{m}$) with approximation to a real polymeric chain ($\boldsymbol{n}$) is limited ($\boldsymbol{m} < \boldsymbol{n}$) by the feasibility of docking in a real-time computational experiment.

Step 3 is extrapolation of the results obtained in steps 1 and 2 to full-length polymeric chains ($\boldsymbol{m} \rightarrow \boldsymbol{n}$) in the search for the most probable modes of the synthetic polymer (ligand)—biopolymer (target) connections and interpretation of the macromolecular interaction mechanism(s).

In order to verify the docking conclusions, a molecular dynamics modelling can be applied additionally. The docking-based interpretation is in need of comparison with experimental results of the known bioactivity (or other properties) of the modelled ligands. If the good correlation is found, this docking approach is applicable and it could be usable for predictive drug design.

Polymeric objects for drug design and modelling

Why polymers may be a promising platform for drug development

Size-inadequacy between small molecular drugs and macromolecular targets of therapy (e.g., proteins)[2] restricts therapeutic potency. Moreover, small molecules, connecting over a small part of the target without any interaction with the majority of the macromolecule, facilitate **drug resistance**. Drug binding can be lost through a simple one-point mutation of the biopolymer target. This loss of drug effect is a real problem in modern prevention/therapy of lethal and rapidly mutating microorganisms, such as **HIV-1,** the causative virus of **acquired immune deficiency syndrome** (**AIDS**) [20]. Under this pathogenesis a

[1] The quantity of possible structural conformations for a small molecule reaches 10^{2-3} [10, 11], and this value increases to $\geq 10^{(2-3)\mathbf{N}}$ in polymeric chains, where **N** is the number of small molecular monomer residues in the N-mer chain (the degree of polymerisation).

[2] Biopolymers are nano-scale targets, as a rule.

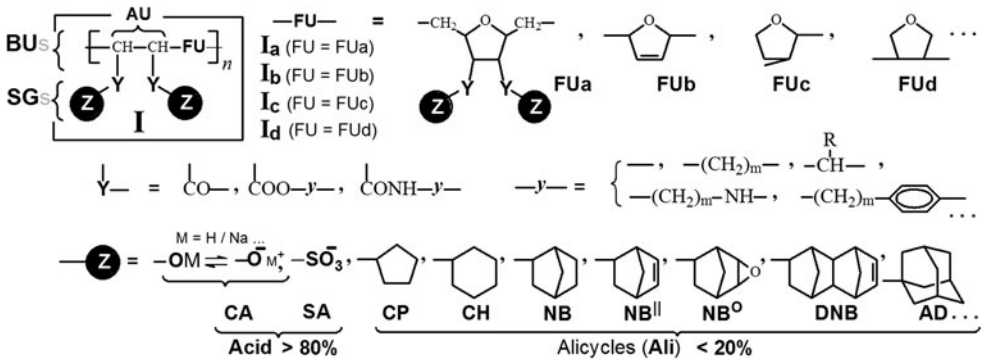

Fig. 1 Synthetic alternating copolymers (I) of maleic acid: with divinyl ether 2:1 (**Ia**), furan 1:1 (**Ib**), 2,3-dihydro- (**Ic**) and 2,5-dihydro-furan (**Id**), heterogeneously modified at the side positions (**Z**) through the bridges (**Y**) by the *anionogenic*: carboxy- (**CA**) and/or sulphoacidic (**SA**) groups, and(or) by the *alicyclic-type hydrophobic* species of cyclopentane (**CP**), cyclohexane (**CH**), norbornane (**NB**), i.e., bicyclo[2.2.1]heptane, norbornan-2-en (**NB**$^{\text{II}}$), 2,3-epoxynorbornan (**NB**$^{\text{O}}$), dinorbornen (**DNB**), i.e., tetracyclo-[4.4.0.$1^{2.5}1^{7.10}$]-dodecene, and adamantane (**AD**), tricyclo[3.3.1.$1^{3.7}$]decene. The chains alternated succinic acid-derived (**AU**) and furan-like (**FU**) co-monomer units

traditional therapy based on only small molecular drugs, vaccination (antibody mediated protection[3]), or even combined therapy, cannot be fully effective [21–23]. The traditional "small molecule" approaches should therefore be complemented by creation of novel drugs responsive on the macromolecular scale.

Within a viral life cycle, small molecular agents are certainly useful as anti-metabolites or virus-specific enzyme inhibitors inside the infected cell, where small molecule metabolites are intensively involved in viral replication. However, extracellular viral particles, so-called virions (**target 1**), as well as key mediators of virus entry (**target 2**), post-replication assembly, maturation and delivery (**target 3**) of next generation virions (**target 4** ~ target 1), represent unique viral nano-aggregates accumulating mostly macromolecules (nucleic acids and proteins). Thus, high molecular compounds should be more effective blockers of **targets 1–4** [7, 24, 25]. The strategy of nano-bio-selective counter-intervention in a viral life cycle by means of hybrid polymeric systems based on the principles of polymer scale adequacy, mimicry (similarity), and complementarity was formulated and experimentally confirmed in our previous research [7]. A new generation of highly effective inhibitors of HIV-1 entry based on a biocompatible synthetic polymer platform were synthesised and evaluated in vitro [7, 12–19]. In this study we consider one series of the synthesised and tested anti-HIV-1 polymer compounds.

Synthetic polymer inhibitors of HIV-1 entry, as macro-ligands

The general topic of the current study was the synthetic polymeric compounds of the generic formula **I** (Fig. 1).

[3] While an antibody is a protein-sized molecule, only small parts of it bind to an antigen directly.

Linear polymeric chains were designed as an alternation of maleic acid monomer units (**AU**) (converted into the chain-coupled succinic acid derivatives) with the co-monomer residues related to furans (**FU**). This artificial alternation of acidic and furan-related (ribose-like) units is similar to the natural nucleic acids backbone, but free of genetically relevant purine/pyrimidine bases. Similarly to the genetic programming of proteins, an artificial programming of the synthetic polymeric chains was regulated through the results-oriented variation of the polymerisation degree (***n***) and the side groups (SG = **–YZ**, non-nucleoside) combinations. These chemical parameters were achieved under controlled conditions of step-by-step synthesis (see experimental section). Specifically, a general excess of the water-ionisable acidic salt groups (**–Y–** = –CO–, **Z** = **CA** or **SA**, >80 %) provided good solubility in aqueous (physiological) media and the optimal safety (cytotoxic concentrations $CC_{50} \geq$ 1,000–2,000 μg/ml, in vitro, and high tolerable doses in vivo) [7, 26]. The completely carboxylic samples (100 % of **Z** = **CA**) inhibited the HIV-1 reproduction moderately [7, 15]. However, **–YZ** modification via varied structures (Fig. 1) significantly influenced anti-HIV efficacy. The resulting IC_{50}, the concentration sufficient for 50 % inhibition of HIV-1 reproduction in cell culture, was decreased to more than a thousand times lower than the 50 % cytotoxic concentration, or CC_{50}. This modulation resulted in notably high selectivity indexes ($SI = CC_{50}/IC_{50}$) of the antiviral inhibition, up to $SI = (3–4) \times 10^3$ [7].

Biopolymeric targets for the studied macro-ligands

Earlier, approximately 170 experimental samples of the series **I** polymers were studied as anti-HIV inhibitors in vitro, in MT4 and Hella cell cultures, in several

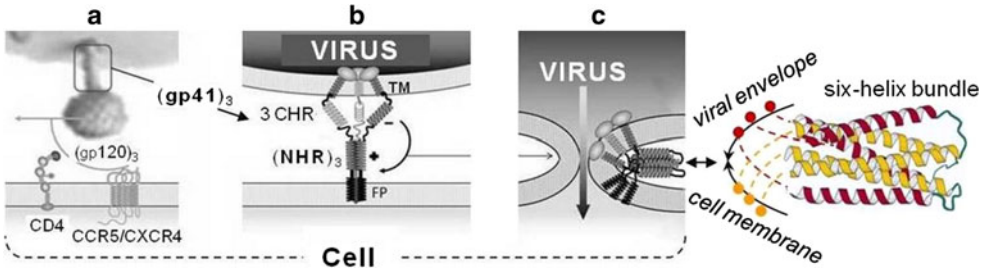

Fig. 2 HIV-1 entry mediators. **a** The **gp120** (triplet composing an external cap on top of the HIV-1 envelope spike) selectively connects with a cellular receptor CD4, and activates (via the V3 loop) binding of the next cell receptor, chemokine receptor CCR5 or CXCR4, as a co-receptor for the virus (with HIV-1 strain R5/R4 tropism). The combined CD4:gp120:CCR5/CXCR4 interaction decomposed the cap, removing the gp120 and exposing the gp41 tri-molecular complex. **b** The C-tail parts of the three **gp41** molecules (including the transmembrane domains, **TM**) are aggregated with the virus, while the N-terminal domains, the so-called fusion peptides (**FP**), penetrate into the lipid matrix of the cell membrane. An aggregation of N-neighbouring "heptad repeat regions" (**NHR,** called also **HR1**) forms the three α-helix $(\mathbf{NHR})_3$ core. This core induces the hairpin co-aggregation of the C-heptad repeat regions (**CHR**, called also **HR2**) toward a coiled-coil six-helix bundle formation. **c** This tri-molecular gp41 six-helix self-collapses and pulls the viral envelope toward the host cell membrane, resulting in fusion. The virion contents can subsequently penetrate into the cell. This figure was drawn based on [27–31]

independent laboratories[4] [7, 12–19]. The following experimental findings were recorded:

1. The tested polymeric agents were not cytotoxic at the tested anti-HIV concentrations;
2. The tested polymers did not directly inactivate HIV-1 extracellular virion infectivity (if the viral media were treated by the polymeric agent with subsequent removing the polymer);
3. The highest inhibition of HIV-1 reproduction was observed when the polymeric agents of series **I** were added to the cell culture no later than 1 h after the virus addition;
4. Addition of polymeric agent simultaneously with the virus resulted in only retardation but not full inhibition of viral adsorption on cell membrane. However, the tested effective concentrations completely blocked penetration of the virus into cells (i.e., no viral proteins/nucleic acids were detected in the cytoplasm/nuclei) [13, 26].

Altogether, these data strongly suggested that the polymers of series **I** selectively blocked a post-adsorption step of the HIV-1 entry, i.e. the fusion. Therefore the most likely targets of these inhibitors are the *viral fusion mediators* [13, 26].

An analytical review of the literature for HIV-1 entry molecular mechanisms leads to the HIV-1 envelope (*env*) glycoproteins gp41 and gp120 as the main molecular machinery for entry (Fig. 2) [27–31].

[4] A. G. Bukrinskaya et al. (Ivanovsky Institute of Virology, Moscow, Russia) I. V. Timofeyev et al. (Centre of Virology and Biotechnology "Vector", Koltsovo, Novosibirsk Region, Russia), E. De Clercq et al. (Rega Institute, Leuven, Belgium), and L. Margolis et al. (National Institute of Child Health and Human Development, NIH, Bethesda, USA) among others.

The gp41 trimolecular object is a key mediator of viral fusion with cell membranes, and the heptad repeat regions, **HRI** (**NHR**) and **HRII** (**CHR**) (Fig. 2), represent crucial targets for fusion blockade by water-soluble inhibitors. Specifically, prevention of pre-hairpin state $(\mathbf{NHR})_3$ tri-helix core aggregation with **CHR** lead to fusion inhibition [32, 33]. Therefore, the $(\mathbf{NHR})_3$ *sub-trimolecular protein-like complex* (and **CHR**) should be considered as the most expected target(s) for the series **I** polymers. This assumption was tested in the subsequent computational modelling.

Materials and methods

Series I polymers synthesis and anti-HIV activity

Synthesis of polymers of general formula ***I*** was carried out in the following three stages. *The first stage* provided polymeric precursors as polyanhydrides suitable for graft-modifications. The alternating copolymers of maleic anhydride with divinyl ether (the precursor for the **Ia** series), furan (for **Ib** series), 2,3-dihydrofuran (for **I**c series), and 2,5-dihydrofuran (for **I**d series) were obtained via the free-radical copolymerisation controlled by chain-transfer agents. *The second stage* was a step-by-step grafting of the required side-group combinations SG = –y–**Z** (SG_F = Z, SG_B = y) by means of partial aminolysis of the precursor anhydride units with H_2N–y–**Z** reagents. *The third stage* included the hydrolysis of the unused aminolysis anhydride units to carboxylic acid semi-sodium salt derivatives (–Y**Z** = –COOM, M = H/Na). The obtained water-soluble products were purified trough a multi-cyclic ultra-filtration and isolated as lyophilised substances. The products were characterised by an element analysis, UV, FTIR, NMR spectroscopy, viscometry, and GPC. More detailed descriptions were published in the previous articles [15, 16, 26, 34] and patents [17, 18].

Anti-HIV activity of the polymeric samples and small molecular controls (rimantadine/amantadine) was evaluated in vitro using MT-4 or TZM-HeLa-CD4 + -LTR/β-gal (**MAGI**) cell lines and various strains of HIV-1. The tested doses of the virus resulted in nearly 100 % death of the cells by the 24th hour after viral addition in the absence of tested compounds (V-control experiments). In the general experimental line, the compounds were added to the cell culture at various concentrations before, simultaneously, or after the virus. The viral entry and reproduction intensity were determined by recording the viral protein/nucleic acid accumulation, as well as cell survival in the general (with compound addition) and V-control (only virus) tests. Detailed experimental techniques, conditions, and data processing were reported previously [15–19]. In section"In silico—in vitro correlation and data interpretation" of this article, the average concentrations for 50 % inhibition of the HIV-1 reproduction ($\mathbf{IC_{50}}$) were used as a measure of the anti-HIV effectiveness. For the Z and EVK viral strains, the IC_{50} values were calculated based on HIV-1 p24 protein levels that were detected by western blot assay. For the HIV-1 899 strain HIV-1 replication was detected by the MAGI indicator cell based single infection cycle assay. Compounds were added not later than 1 h after the virus (1 h is the time of HIV-1 pre-fusion adsorption).

The models and docking

The investigated ligand models corresponding to structural components of the investigated synthetic polymers series **I** within various levels of modelling were named **M1**–**M7**. In case of possible isomeric variability, only confirmed synthetic polymer fragments were used for modelling. For example, based on previous publications [26, 34–40], the –**FUa**– units were modelled as 5-membered (furan-like) cycles with cis-methylenes in the 2,5-positions, methylenes trans to neighboring carboxylic groups (2,3- and 4,5-positions), and cis carboxylic groups (3,4-positions).

The starting coordinates for the atomic positions of the trihelix $(\mathbf{NHR})_3$ core were obtained from PDB (1aik for the native gp41 and 1f23 for the I573T mutant gp41). For modelling the ligands molecular-graphic package SYBYL 8.0 [41] was used, and for creation of the $(\mathbf{NHR})_3$, both SYBYL 8.0 and Swiss-PDBViewer software were employed [42]. The models optimisation and removal of unfavourable van der Waals interactions within the $(\mathbf{NHR})_3$ structure were performed by short minimizations using SYBYL 8.0 and Powell's method [43] with the following parameters: TRIPOS force field [44], non-bonded cut-off distance equal to 8 Å, a distance-dependent dielectric function, the simplex method in an initial optimisation, and a termination cut-off equal to 0.05 kcal/(mol × Å). For calculation of partial atomic charges for the ligands, the quantum–mechanical semiempirical method PM3 [45, 46] was applied using the package MOPAC 7.0 [47] included in the package Vega ZZ [48]. To estimate partial atomic charges for the $(\mathbf{NHR})_3$ atoms, the Gasteiger-Huckel method [49] was applied through SYBYL 8.0. To define the probable binding sites on the $(\mathbf{NHR})_3$, the docking of flexible ligands to the rigid $(\mathbf{NHR})_3$ full surface was carried out with the programme package DOCK 6.4 [50]. The method used by DOCK generates a set of overlapping spheres that surround target and touch its solvent-accessible surface at only two points. Therefore, the solvent-accessible surface for $(\mathbf{NHR})_3$ was calculated using the Connolly algorithm [51] with a probe radius of 1.4 Å and using routine DMS [52]. Prior to docking for the binding energy score, the electrostatic and van der Waals potential fields in the nodes of a grid covering a 3D box containing the target were calculated under the following parameters: a grid cell size equal to 0.3 Å, a non-bond cut-off distance of 12.0 Å, and the van der Waals interaction parameters were used from the dw_AMBER_parm99.defn set. This grid-based energy score was applied for minimisation of the ligands after an initial placement in the docking site. Flexibility of the ligand was modelled by treating the ligand as a series of fragments, where a central fragment (the anchor) was docked first and followed by sequentially docking the outer fragments around the anchor [53]. The best conformer was selected based on the secondary scoring function of DOCK, which applied the generalised Born approach with solvent-accessible surface area (GB/SA) based on the algorithm of Hawkins et al. [54]. In this approach salt (NaCl) screening electrostatic interactions were at the 0.1 M concentration. For searching the score mode most correlated to the in vitro experimental data, the consensus approach was applied based on combinations of the above-mentioned secondary scoring function of DOCK with the Sybyl package CSCORE module (D-Score, G-Score, ChemScore, and PMF).

Results and discussion

Target characterisation and modelling

In earlier publications, either gp41 $(\mathbf{NHR})_3$ or **CHR** were investigated and characterised as targets for the local effect of small molecules [32, 33, 55–57], polypeptides [32, 33, 58], and antibodies [59] without an analysis of the attraction potential of the objects to anionic polyelectrolytes, such as the synthetic copolymers **I**. However, useful preliminary information about the $(\mathbf{NHR})_3$ and **CHR** relative potentiality to be an expected target could be predicted based on their amino acid sequence organisation analysis. A scheme for the **NHR** and **CHR** regions arrangement is shown in Fig. 3 (based on [27, 28, 60–65]).

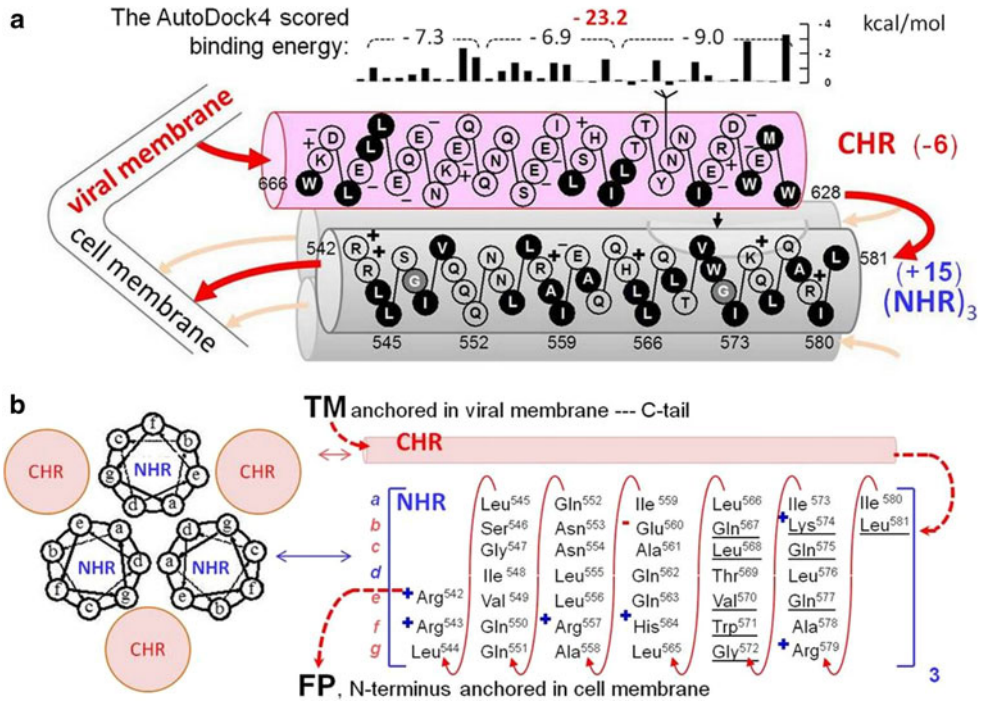

Fig. 3 The NHR and CHR amino acid sequences and arrangement for aggregation. **a** The scheme for the **CHR** approaching to the $(\mathbf{NHR})_3$ (only one of three **CHR** helices is shown). Amino acid sequences of both regions conform to the repeated heptads leading to α-helix formation. The shown binding energy of the **CHR** with $(\mathbf{NHR})_3$ was extracted from the previously published data [64, 65]. **b** The $(\mathbf{NHR})_3 + 3$ **CHR** co-aggregation scheme, as viewed from the cell (gp41 N-terminus). The **NHR** amino acid sequence in order of the repeated heptads **a**-**g** is shown in the table (right): the **a** and **d** positions provide the **NHR** triplet interconnecting in the $(\mathbf{NHR})_3$ core, and the positions **b**, **c**, **e**, **f**, and **g** form an interface for the external environment, including interaction with **CHR**s. Note: the ionisable residues are marked by **+** or**—**(corresponding to the charge), and the hydrophobic residues are displayed in the black (Fig. 3a). This figure was drawn based on [27, 28, 60–63]

Each of the three identical and parallel **NHR** α-helices contains an excess of basic residues ($Arg^{542,543,557,579}$, Lys^{574}, and His^{564}) in comparison with acidic residue (Glu^{560}). This ratio predetermined the excess of positive charge under ionising conditions in aqueous media up to +5 per one helix and +15 per $(\mathbf{NHR})_3$ core. On the contrary, the **CHR** has an excess of acidic residues ($Glu^{630,634,647,648,654,657,659,662}$, $Asp^{632,664}$) in comparison with the basic residues (Arg^{633}, $Lys^{655,665}$, His^{643}), and the CHR is capable of accumulating the excess of negative charge up to −6 per **CHR** helix. Therefore, the **NHR** and **CHR** regions represent poly-cationic and poly-anionic blocks, respectively, that can assemble into the [$(\mathbf{NHR})_3 + 3\mathbf{CHR}$] complex.

Similar to **CHR**, the synthetic copolymers **I** (Fig. 1) also represent the acidic chains that are ionized (at physiological pH) possessing the negative charge. Due to coulombic forces the ionized copolymers **I** will attract the **NHR** helix or $(\mathbf{NHR})_3$ core but repulse the **CHR** regions. Thus, the anion-electrostatic nature of the copolymers **I** defines their selective affinity to the $(\mathbf{NHR})_3$ but not to the **CHR**. Similar selectivity can be predicted by comparing their hydrophilic-hydrophobic balance: the **NHR** is more hydrophobic than **CHR** [60] (48 and 28 % hydrophobic amino acids, respectively). In this respect, the water-soluble copolymers **I** chains (Fig. 1), non- or moderately modified by hydrophobic alicycles, also imitate the **CHR** chains, and additional grafting the alicycles to the chains should increase in hydrophobic tropism toward the $(\mathbf{NHR})_3$ counter-partner but not to the **CHR**.

For the above-mentioned reasons, we focused on the copolymers **I** as the macro-ligands most likely to bind $(\mathbf{NHR})_3$.[5] This is similar to viral **CHR** targeting, but copolymers are competing with the **CHR**.

The $(\mathbf{NHR})_3$ 3D model derived from the PDB ID:1aik file is presented in Fig. 4. The target overall dimensions are 5.1 × 2.5 nm, indicating a nano-object. As the unidirectional alpha-helix trimer, the $(\mathbf{NHR})_3$ possesses the 3-fold rotational symmetry (C_3), reproducing a geometry and characteristics of own structure with rotation by every 120° (around the C_3 symmetry axis). The target consists of three levels (**L-1**, **L-2**, and **L-3**) of cavities between the adjacent

[5] This assumption has been verified by a test-docking of the **Ia** derived models (see below) to the both **NHR** and **CHR**. The **NHR** possessed significantly more (than **CHR**) multiplicity and higher binding energy (1.5–2 fold stronger).

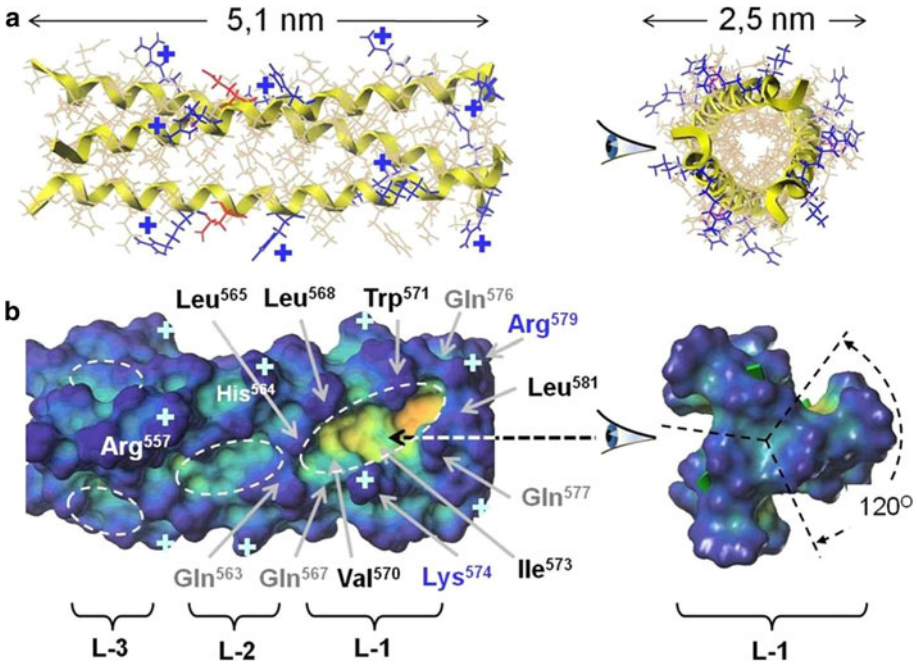

Fig. 4 **3D organisation of (NHR)$_3$** . **a** Ribbon model: views along (left) and from C-tail (right). The **+** labels the basic amino acids. **b** Surface of the target displayed in depth gradation (from blue to yellow). Three levels (**L-1**, **L-2**, and **L-3**) of cavity triplets take place around the target. Amino acids surrounding one of the three major (and identical) cavities (often designed as "pockets") within **L-1** are shown in detail. The **L-1** pockets and smaller cavities of **L-2/L-3** areas are outlined with a dotted curve

NHR α-helices. At every level around the target, the corresponding size cavity repeats itself three times (Fig. 4).

At the border of the each of three main cavities (commonly termed ***pockets***) on the **L-1** level (Fig. 4b) the hydrophilic and ionisable to positive charge amino group of lysine (Lys^{574}) is present. The amide termini of the glutamines (Gln^{563}, Gln^{567}, and Gln^{577}, the hydrophilic donors and acceptors of H-bonds) are located near to the Lys. On the opposite side of the pocket a row of hydrophobic side chains (aliphatic hydrocarbons of the Leu^{565}, Leu^{568}, and Leu^{581}, and the indole of the Trp^{571} residue) are situated. The **L-1** (amino acids 565–581) range of the (**NHR**)$_3$ pockets plays a key role in binding the **CHR** via amino acids 628–634 locus, enriched with acidic and hydrophobic residues [66]. Comparative contributions of different levels to the binding energy per single **CHR** could be estimated from the docking (AutoDock4) data reported earlier by Ramirez [64] and Gaston [65] (Fig. 3a):

L-1		**L-2**		**L-3**	
|-9.0|	>	|-6.9|	≈	|-7.3|	*total of* **−23.2** *kcal/mol per single* ***CHR*** (1)

The considered 3D model of (**NHR**)$_3$ derived from the PDB ID:1aik were explored previously by many researchers in searching for HIV-1 fusion inhibitors. For this purpose, a molecular docking approach has been applied widely, although predominantly for small molecule ligands targeted to the **L-1** of pockets [32, 33, 55–57]. Meanwhile, the extended binding potential of synthetic polymeric compounds [7] had not been studied. Focusing the only pocket locus limits a completeness of the target exploration; therefore many possibilities for additional polymer-cooperative blocking contacts, for example, on less deep cavities of the **L-2/L-3** levels (Fig. 4) have not been considered.

Synthetic polymers modelling and docking to the target

The modern computational powers and current docking software do not allow for modelling of a synthetic macromolecule as an entire ligand because of the immense conformational capacity. Therefore, we suggested the special algorithm for this task (see "The docking strategy proposed for polymeric macro-ligands" section) and applied it for the synthetic copolymers **I**. Within the scope of the declared strategy, a multilevel modelling of structures **I** was performed with application of the following 7-level (M1–M7) algorithm of sub-molecular model linkages (Fig. 5).

The models M1, M2, and M3 (Fig. 5) simulated the separate polymer components: *backbone units* (BU = M3), multi-repeated along the polymeric chain, and variable *side groups* (SG = M1 and M2, where M1 = SG$_F$ and M2 = SG$_F$–SG$_B$). These models corresponded to **step 1** of the proposed docking strategy. And the models M4–M7 were used in **step 2**, the docking of component-integrating models.

Step 1: separate polymer components (M1–M3) docking

The terminal (functionally active) *fragments of side groups HZ (models **M1**)* are the simplest models without consideration of any bridges or polymer backbone units. The **M1** models of the alicycle series (**ZH** = **Ali,** see Fig. 1) widely spread themselves on the target surface, preferably near the hydrophobic sites of the main pocket triplet of the **L-1** level, as well as on the **L-2** and **L-3** levels of the less deep cavities (Fig. 6a). The minimum free energy values were calculated in the pocket locus near the hydrophobic Trp^{571}, and the binding potency was ranked in the following order:

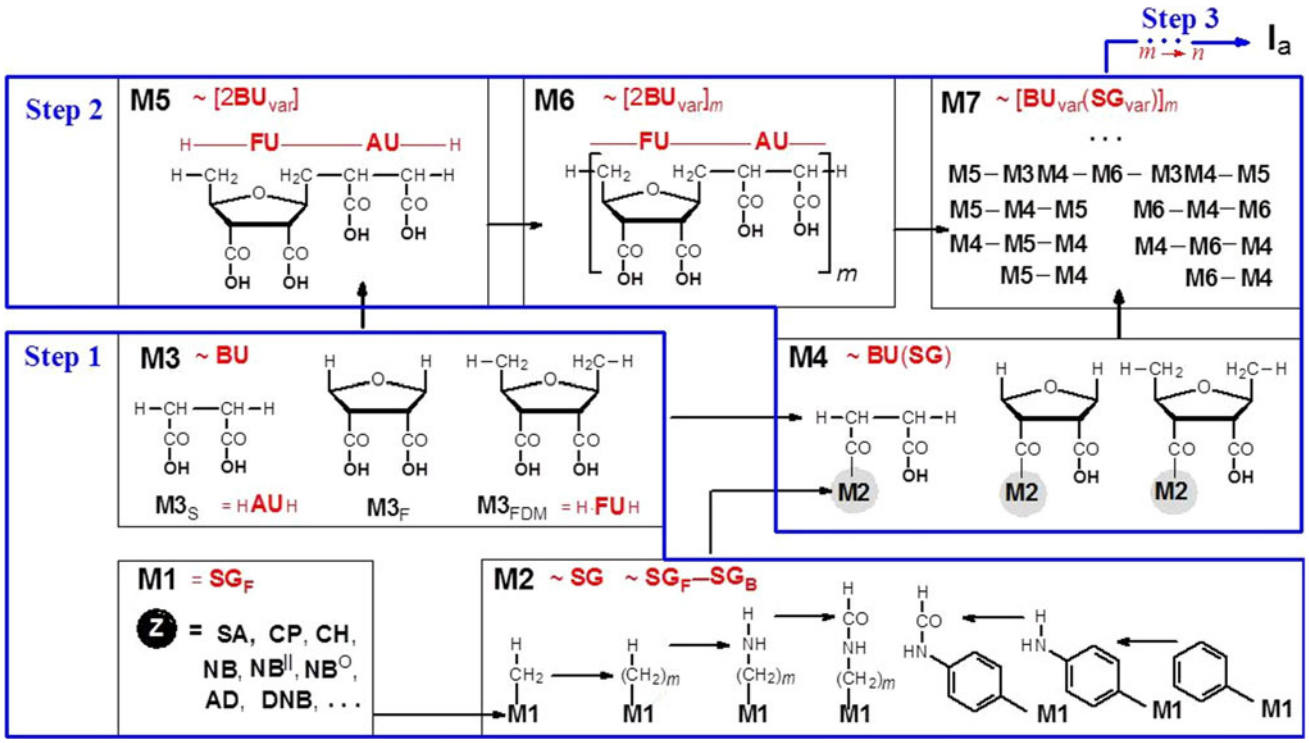

Fig. 5 Sub-ligand modelling levels of the Ia copolymers series **M1** = ZH—the terminal functionally active fragments of the side groups; **M2** = M1 + atomic sequence of a bridge toward the polymeric chain backbone = ZYH; **M4** = M2 + a single fragment of the polymer backbone, H–**AU**-H = HCH(YZ)-CH(YZ)H, or H–**FU**–H; **M3** = a single fragment of non-modified backbone from **M4** (where –YZ = –CO**CA**, 100 %); **M5** = full co-monomer unit of the unmodified polymer backbone, H–**AU**–**FU**–H = CH_2(YZ)-CH(YZ)**FU**H (where –YZ = –CO**CA**, 100 %); **M6** = $[M5]_m$, m = *2*, 3, 4, …—chains of unmodified backbone units (oligomers); **M7** = the oligomeric chains heterogeneously modified by varied combinations of side groups -YZ

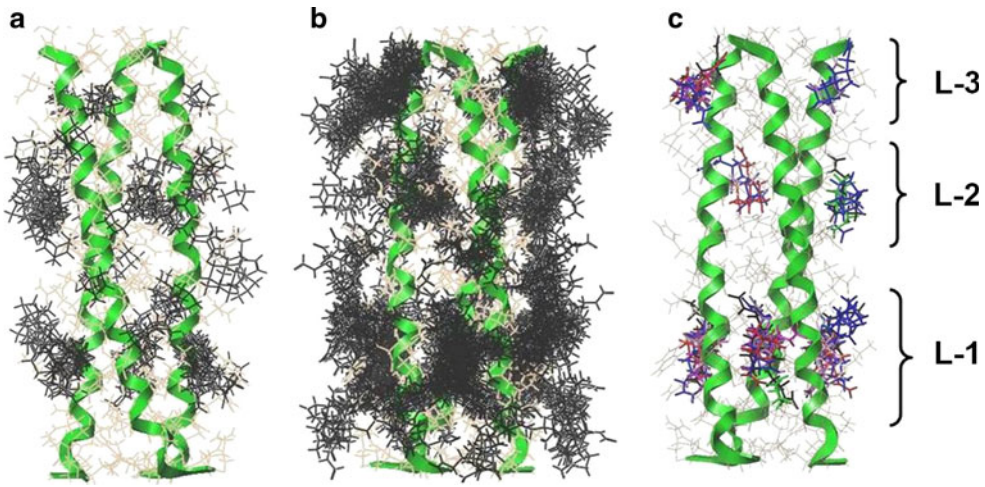

Fig. 6 The M1 and M2 series models docked on the $(NHR)_3$ surface a M1 series models of sub-ligands with Z = all variations of **Ali** (124 docking outputs). **b M2** models = ZYH, where –Y– = $–(CH_2)_{0\text{-}3}NHCO–$ (1,342 docking outputs). **c** The 10 best by binding energy outputs for every kind of **Ali** selected in **b**

L-1 *level*													
DNB		AD		NB^{o}		NB		$NB^{\|}$		CH		CP	
|-18.7|	>	|-16.6|	≈	|-16.8|	>	|-15.1|	=	|-15.1|	>	|-13.8|	>	|-12.7|	*kcal/mol*

(2)

This order in comparison with the above-mentioned (1) **CHR** binding energy within the same **L-1** level (|−9.0| kcal/mol) allowed one to assume there were good preconditions for a competition between the **CHR** and the tested alicyclic anchors for binding to the pocket. Thus, the **DNB/AD/ND**-type structures were selected from among the docked models as more preferred binding candidates than the **CH/CP**.

While considering the other levels (**L-2** and **L-3**) of the less deep cavities, we ascertained that these niches were also potentially capable of competitive binding via the alicyclic anchors with lower but significant binding strength (60–70 % of **L-1**). This additional capacity could be reasonably rejected under routine screening of small molecules, but in this study we dealt with the polymer-integrative perspective.

*The side groups with bridge fragments HYZ (model line **M2**)* allowed estimation of the partial contributions of the bridges, **Y**, linking **Z** with the polymer backbone (but without the backbone itself considered). Generally, the **Y** bridges did not destroy the above-mentioned positioning of the alicyclic **Z** on the three **L1-L3** levels of the target pockets/cavities (Fig. 6b, c). The methylene ($–CH_2–$) units of **Y** serve as bridge "flexibility hinges", moderately influencing the binding energy, while the more polar and rigid amide fragments (–NHCO–) contributed to this energy more because of their coulombic forces. The considerable negative charge accumulated on the oxygen atom played an important role in interactions with local positive charges near the nitrogen atoms of the target structure, specifically Lys^{574}, $Gln^{563,567,577}$, and Arg^{579} in the pocket. According to the docking results, these contacts were suitable for H-bonds formation.[6] The binding energies[7] in the pocket region of the target for the **M2** line model examples (where $–Y– = –CH_2NHCO–$) are shown in Table 1.

A substitution of the alicyclic **Z** = **Ali** with the sulphonic acid anion **Z** = SO_3^- (**SA**) in the models of series **M2** did not change their general distribution on the three **L1**-**L3** levels of the target surface (where the **L-1** pocket level stayed the most preferable docking area). However, the anionic species significantly influenced the priorities of the local binding contacts. Within the pocket area, the SO_3^- anions of the **M2** = H**Y**–**SA** models (unlike H**Y**–**Ali**) were concentrated around the cationogenic Lys^{574} and Arg^{579}, relocating the amidic and hydrocarbon units of H**Y**-bridges toward the centre of the cavity. The –NHCO– fragments were subsequently able to find contacts with amidic groups of the $Gln^{563,567,577}$, and hydrocarbon fragments could interact with the hydrophobic $Leu^{565,568,581}$ or Trp^{571}. In general, HY-**SA** models possessed binding energies 7–10 kcal/mol less than the HY–**Ali** models, if they contained similar bridges.

*The carboxylic acid fragments of polymer backbone monomer units (models **M3**)* were also concentrated near to cationogenic amino acids of the target, near Lys^{574} or Arg^{579} (on the **L-1** level of the pockets) preferably, and near His^{564} and Arg^{557} (on the **L-2** and **L-3** levels of the target cavities) to a lesser degree.

Step 2: docking of the component-integrating models M4–M7

*The carboxylic acid co-monomer units (models **M5**)* possessed behaviour similar to the models **M3**.

*The carboxyacidic oligomeric chains of the polymers (models **M6**)* also covered the target **L-1** level pockets, but extended over the pockets too, mainly in axial directions between the parallel α-helices of the target (Fig. 7). One of the **M6** model covered one of the three pockets, and similarly the other two pockets could be covered simultaneously by another two of the **M6** model chains. Thus, during interaction with the $(\mathbf{NHR})_3$ target, the negatively charged polycarboxylic chains demonstrated behaviour similar to one of the viral **CHR** helices (possessed the same charge). Both **M6** and **CHR** were self-oriented to an axial aggregation with the $(\mathbf{NHR})_3$ along and between pairs of the **NHR** α-helices.

Unlike the pure alicyclic **M1** models, the poly acidic **M6** models were capable of forming H-bonds, and in contrast to the –NHCO– bridge fragments of the **M2** models, they were capable of ion-salt bonding with positively charged

[6] The Dock6 results accept the H-bond formation (within the 3 atoms X_D, H_D, and X_A) if the following two conditions are met: (1) the distance between H_D and X_A is less than or equal to 2.5 Å; (2) the angle defined by X_D, H_D, and X_A is between 120° and 180°. Several score functions are able to recognize the possibility of H-bonding directly, for example, the G-Score and ChemScore algorithms include direct calculations for the H-bonds contribution in ligand-target binding energy.

[7] Including a solvation effect score.

Table 1 The minimums of the **M2** = **Z**–CH_2NHCOH energies for binding with the $(\mathbf{NHR})_3$ target

The **Z** type in **M2**	**NB**	**NB**$^{\|}$		**NB**^{O}	**DNB**	**AD**
Energy, (kcal/mol)[a]		*exo*	*endo*			
$\mathbf{E_{MM\ MM\ GB/SA}}$ (Δ)	**−22.0** (−6.9)	**−20.9** (−5.8)	**−20.2** (−5.1)	**−22.6** (−5.8)	**−23.2** (−4.5)	**−21.4** (−4.8)
Including the VdW	−22.5	−22.3	−20.6	−23.8	−23.7	−21.4
C + S	3.9	4.9	3.8	1.6	4.3	3.5
SAS	−3.4	−3.4	−3.4	−3.5	−3.7	−3.5

[a] $\mathbf{E_{MM\ GB/SA}}$—the MM GB/SA scored values. In brackets—the decrease in binding energy in comparison with binding energy of the precursor **M1** models. Below the partial contributions in $\mathbf{E_{MM\ GB/SA}}$ are shown: **VdW**—van der Waals forces, **C + S**—coulombic forces with solvation effects, and **SAS**—solvent-accessible surface effects

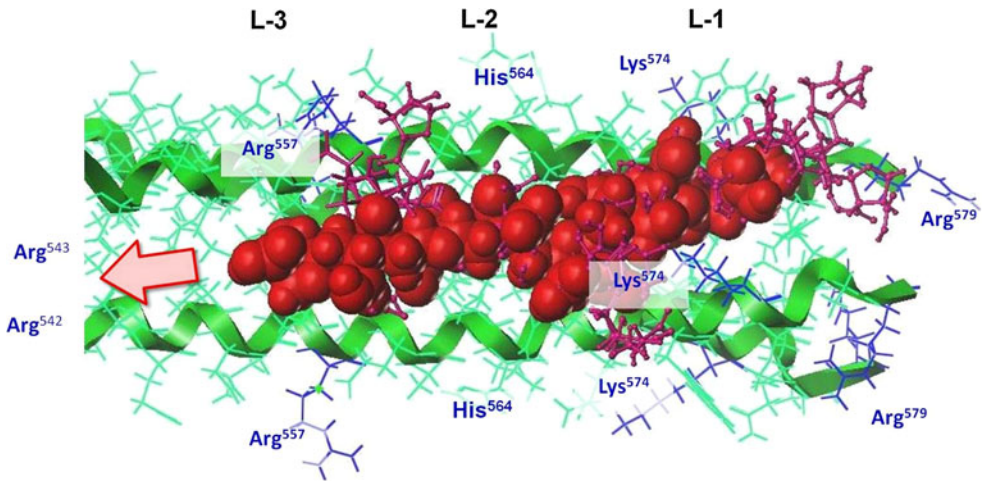

Fig. 7 The fully polycarboxylic (Z = CA, 100 %) oligomeric M6 model docking The **M6** chain orients itself predominantly to an axial aggregation with the $(\mathbf{NHR})_3$ along and between pairs of the **NHR** α-helices. The five conformers of **M6** = H–[–**FU**–**AU**–]$_3$–CH_3 are displayed (*dark red*: four by ball and stick, and one by space fill representation). Minimum binding energy was scored as—30.3 kcal/mol

side chains of the target amino acids. This provides additional points for bonding/fixing the synthetic polycarboxylic chains both inside the pocket locus and outside, along the **NHR** helices (in order of the sequence: Arg^{579}, Lys^{574}, His^{564}, and Arg^{557} with extrapolation toward the Arg^{543} and Arg^{542}). The docking-based calculations of the binding energy minimums for the carboxylic **M3**, **M5**, and **M6** models in varied chains length are indicated in Table 2.

The data represented in Table 2 demonstrate fundamentals of the polymeric state. Non-additive increases in the binding energy, while increasing chain length indicated that the monomer fragments integration in polymeric chain constrained the mobility of every single fragment (unit) of chain to be spacial free for individually optimal contacts with the target. However, the chain-mode co-linking these fragments together leads to the *cooperative multi-point binding* with the target, resulting in increased total binding energy. Starting from the carboxypolymeric chain **M6** model, the binding power increased up to |−30.3| kcal/mol, greater than the power of the viral **CHR** polypeptide chain (|−23.2| kcal/mol).

Table 2 The minimum binding energies of the **M3**, **M5**, and **M6** models to $(\mathbf{NHR})_3$

Model \ energy, kcal/mol[a]	$\mathbf{E_{MM\ GB/SA}}$	VdW	C + S	SAS
M3 = CH_3–**AU**–CH_3	**−14.2**	−15.9	4.5	−2.7
H–**FU**–H	**−17.3**	−18.5	4.5	−3.2
M5 = CH_3–**AU**–**FU**–H	**−19.6**	−27.5	12.0	−4.1
M3M5 = CH_3–**AU**–**FU**–**AU**–CH_3	**−17.1**	−15.7	2.0	−3.4
H–**FU**–**AU**–**FU**–H	**−20.5**	−32.2	16.3	−4.6
M6 = H–**FU**–**AU**–**FU**–**AU**–**FU**–**AU**–CH_3	**−30.3**	−50.1	26.0	−6.2

[a] $\mathbf{E_{MM\ GB/SA}}$—the MM GB/SA scored values. Below the partial contributions in $\mathbf{E_{MM\ GB/SA}}$ are shown: **VdW**—van der Waals forces, **C + S**—coulombic forces with solvation effects, and **SAS**—solvent-accessible surface effects

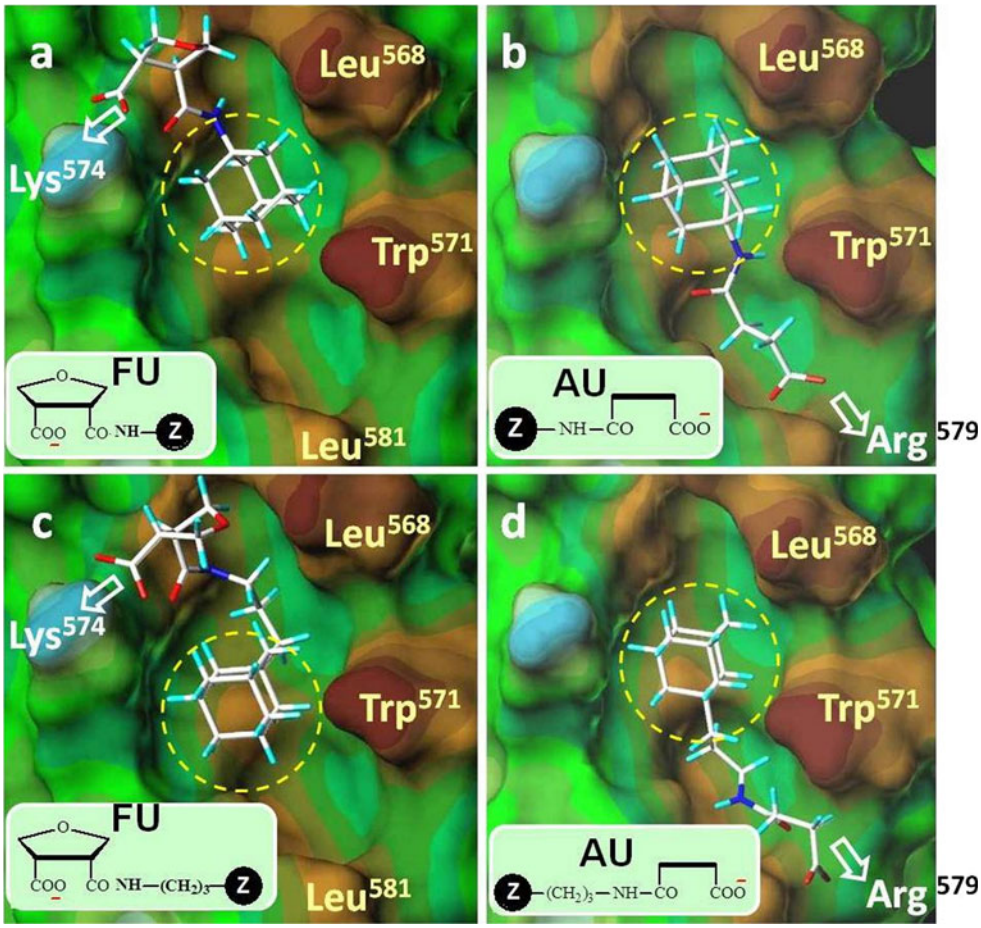

Fig. 8 Examples of M4 models (in the shown structures) docking orientations in the target pocket

The models integrating the backbone units with the ***Z*** *side groups through the –**Y**– bridges (models **M4** or **M7**)* were notably useful for revealing certain interesting nuances of possible antagonism or synergism of the different[8] units, groups and bridges in interactions between themselves or with the $(\mathbf{NHR})_3$ target. In addition, molecular structure factors determining chain fragments locations/orientations on the target became more clear. For example, in the pocket area alicycles (**Z** = **NB**, **NB**$^{\mathrm{I}}$, **AD**, **DNB**) targeted to the hydrophobic Leu^{568} and Trp^{571}. The acidic groups (**Z** = **CA** or **SA**) were oriented in the opposite direction toward the cationogenic amino group of Lys^{574} (Fig. 8) or the guanidine group of Arg^{579}. As a result, if the polymeric chain unit is modified by sulphonic acid side groups, these groups compete with carboxylic acid groups for cationogenic amino acid residues.

On the contrary, the alicycles, as hydrophobic anchors, did not compete with the carboxylic groups. The alicycles found additional points for binding with hydrophobic $Leu^{565,\ 568,\ 581}$ and Trp^{571} within the pocket locus.

[8] Different by chemical nature and of location in the macromolecule.

It was interesting that the chemical structure of the backbone unit to which the **Z** = **Ali** was linked (by a bridge) regulated a local orientation of docking to the target. In the case of the **Ali**-type anchor linked to the **FU** (furan-derived) unit of the polymer backbone, the carboxylic group in the same unit was oriented toward Lys^{574} and the **Ali** was located near Leu^{568} and Tpr^{571} (Fig. 8a, c). However, if the **Ali** was linked to the **SU** (succinic) unit of the backbone, the **Ali** anchor kept its location, while the direction of the carboxylic end switched toward Arg^{579}. A variation in length of the linking bridge –**Y**– = $–(CH_2)_mNHCO–$ in the range of m = 0–3 did not affect the noted model orientation significantly, and the inserted $–CH_2–$ motifs only occupied a space vacancy in the pocket (Fig. 8b, d). The position of the **Ali** anchor grafting to the particular (ether **FU** or the **AU**) unit of the polymeric chain backbone could thus regulate the orientation of the **M4** models in the pocket. It must be noted that the observed orientation anisotropy conformed with the pocket geometry: the access to Arg^{579} was controlled by the local groove between Trp^{571} and Leu^{581}, which was too narrow for penetration of the **FU** unit but not the **AU** unit (more compact and flexible) (Fig. 8).

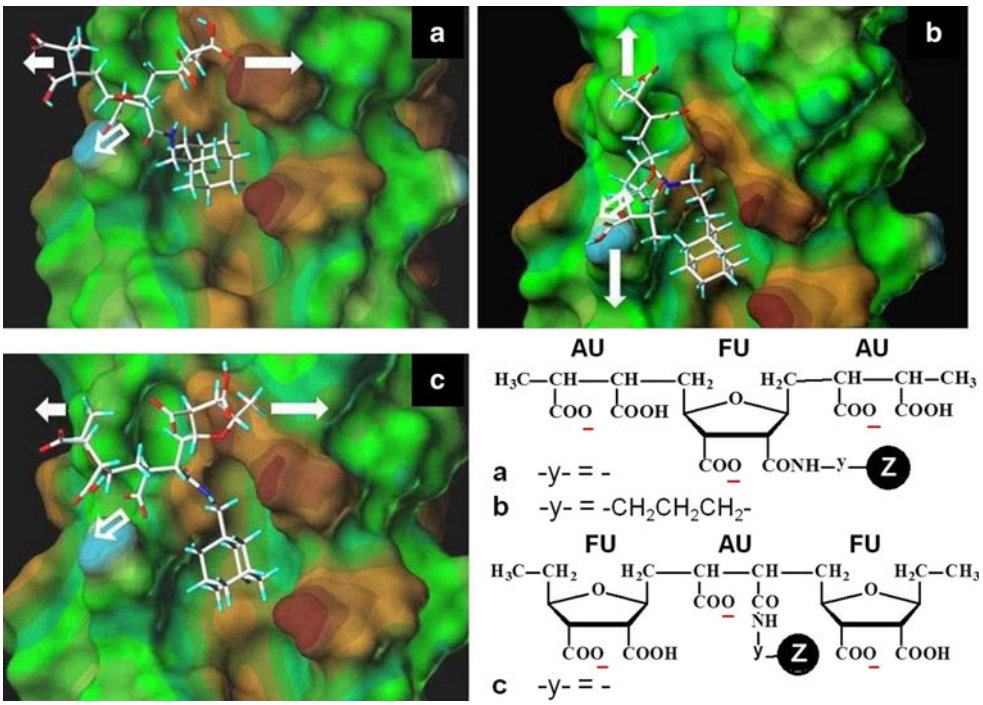

Fig. 9 The results of docking the extended models M4M5M4 in the shown structure (Z = AD)

However, in the real polymeric molecules, each single unit of backbone is linked with adjacent units forming a polymeric chain. In the case of the **Ia** series copolymers, we dealt with the linear-chain alternation of the **FU** and **AU** units as positions for variable anchors grafting along the chain. In such a situation, it was necessary to continue the modelling to understand the role of anchors and bridges in the regulation of the chain orientation. This step involved linking the **Ali** anchor-modified units with extended motifs of the **Ali**-free polymeric chain units. The above considered **FU**(SG) and **AU**(SG) models were enlarged to –**AU**–**FU**(SG)–**AU**– or –**FU**–**AU**(SG)–**FU**- models, as illustrated in Fig. 9.

As result of docking, the following data were obtained. The **AD**-modified **FU** unit integrated with two **AU** terminal units held the acidic groups near Lys^{574} (Fig. 9a, b). However, the anchor-modified **AU** unit integrated with two **FU** terminal units lost a priority to location near Arg^{579} reorienting also toward Lys^{574} (Fig. 9c). Therefore, the **AU** unit could not adapt to the narrow groove to reach Arg^{579} because of steric bulk of flanking **FU** units. A docking study of the considered models clarified how the bridge length influenced orientation of the extended chain motif anchored in the pocket. The models with short bridges (-y- = -) preferred diametrical orientation (Fig. 9a, c), whereas the models with extended bridges reoriented in the axial direction with respect to the $(\mathbf{NHR})_3$ target (Fig. 9b). A dramatic significance of this switch of orientation will be considered bellow.

The models of modified oligomeric chains (models **M7***)* satisfied maximum "modern docking permitted" for the approximation of the model to the synthetic polymer chains (or to notably large in size different parts of the chains). This model series allowed extensive integration of single monomer units and side fragments toward the representative polymer chains with combinatorial modelling. The modelling also account for various side groups **Z** (or combinations), bridges, degree of polymerisation (***m*→*n***, determines the chain length),[9] and positioning of the side groups along the chain. These complex and flexible models required flexible docking technique (see "The models and docking" section).

The first group of the **M7** models represented an augmentation of the polymer chain sequence from –**AU**–**FU**(Y**Ali**)–**AU**– (Fig. 9) to the **M7** = CH_3[**AU**–**FU**][**AU**–**FU**(Y**Ali**)][**AU**–**FU**]H, where the **FU**(Y**Ali**) is an **Ali** anchor-modified furan-like unit of backbone. Docking such **M7** models to the $(\mathbf{NHR})_3$ target confirmed the dependence of the chain orientation on the anchor-linking bridge length (Fig. 10, a—short bridge, b—bridge elongated by three methylene insertions). However, every next unit addition to the chain termini made the both termini more independent of the anchor-containing central unit and more mobile. For extended chains, the presence of more than one anchors and certain distance between them were necessary for specific binding orientation on the target surface. Particularly, the **Ali** anchor grafting to every 3rd or 4th co-monomer unit (–[**–FU–AU–**]–) of the chain conformed

[9] In this study we experimentally modelled the chains up to pentamers by alternating the five furan-like and succinic acid derived units.

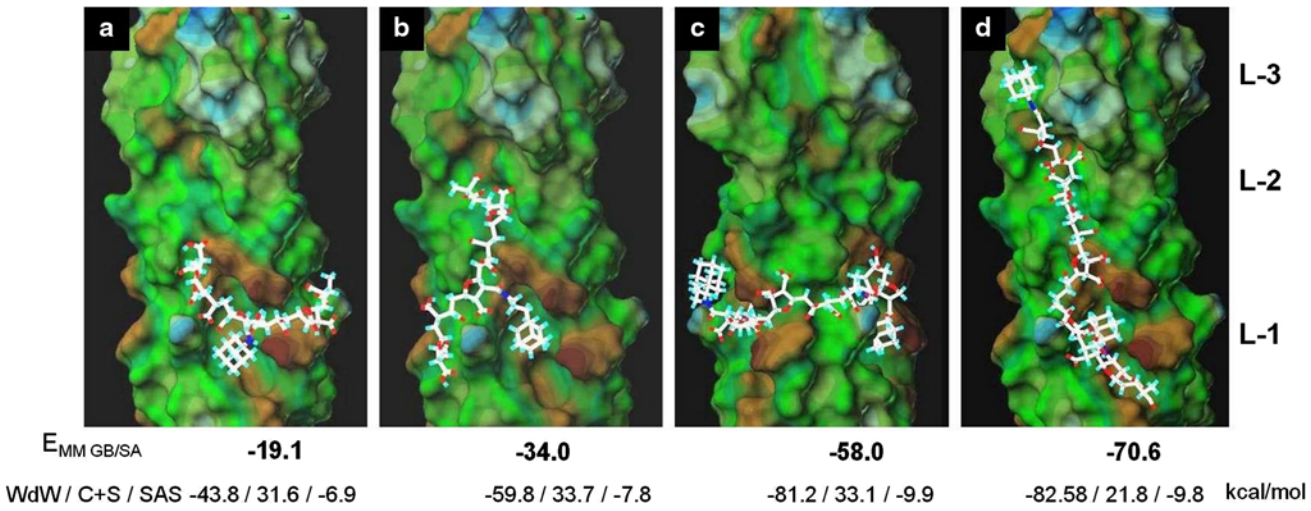

Fig. 10 **M7 models docking results a** and **b:** full co-monomer trimers with a single anchor (Z = **AD**) grafted to the furan-like section of the central co-monomer unit through different –CONH$(CH_2)_m$– bridges; **a** (m = 0) and **b** (m = 3). **c** and **d**: full co-monomer tetra- and pentamers, correspondently, modified with two **AD** anchors at both termini through similar bridges (–CONH$(CH_2)_m$–)

with the belting distance between two pockets of the target. Models **M7** of this category were distinct by having predominantly belting conformations around the (**NHR**)$_3$ target, mainly from pocket to pocket within the L-1 level (Fig. 10c), in contrast with axial positioning typical for the anchors-free **M6** models (Fig. 7). However, subsequent increases in the distance between the anchors reversed the chain orientation back to axial (Fig. 10d). The first anchor remained at the **L-1** pocket, and the second was relocated along and between the **NHR** α-helices up to the **L-3** level cavity (Fig. 10d). Such behaviour correlated with the binding capacity of the **Ali**-type **M1/M2** models toward both **L-1**, and the **L-2/L-3** levels of cavities (Fig. 6).

The results obtained from docking indicated that unlike the helix-structured polypeptide-type CHR chains of the viral gp41 molecules, the flexible chains of the modelled synthetic polymers series **Ia** were much more adaptable to the (**NHR**)$_3$ surface in various directions. A switch from the axial to the belting mode of binding to (**NHR**)$_3$, and inversely, could be regulated by the alicyclic anchors considered here.[10]

In silico—in vitro correlation and data interpretation

Previously obtained experimental (in vitro) data for HIV-1 entry inhibition by the 170 samples of the **I** series copolymers were partially reported in previous publications [7, 13–18, 67, 68] and reviews [26, 69]. The most representative current results are presented in Table 3.

"Chemical structure—binding energy—anti-HIV-1 effectiveness" correlation

For analysis of the in vitro and in silico data in relation to the chemical organisation of **Ia** copolymers, the following two categories of the molecular structure factors should be taken into consideration. The first category is identically constructed [–**AU**–**FU**–]$_n$ units of the polymers backbone (the constant part), and the second is regulated combinations of side-groups/anchors (-Y**Z**) variable by structure, contents, and positioning along the chain (the variable part). In this regard, the crucial factors of the "functionality—effectiveness" differences from one sample to the next should be looked for in the variable part. For this part modelling begins from the start step models, **M1** (H**Z**) and **M2** (HY**Z**).

The anti-HIV-1 effectiveness of the polymeric compounds **I** in comparison with the energies of **M2** models binding with the (**NHR**)$_3$ are represented in Table 4. The comparative analysis of the biological (in vitro) and computational (in silico) experiments data revealed a high correlation.[11] This correlation was maintained through the levels of modelling up to the **M7** = CH_3[**AU–FU**][**AU–FU**(–Y**Z**)][**AU–FU**]H. The following order of priority of the **Ali** anchors was found both in vitro and in silico:

[10] Other types of anchors will be reported in future publications.

[11] This correlation degree depends on scoring algorithms of the docking results to a certain extent, and one of the top correlations was obtained with ChemScore function. It can be related to a more adequate scoring of the contributions [70] from not only H-bond forces, and rotation entropy but also from the lipophilic effect, which is typical for hydrophobic **Ali** -structures of the considered anchors.

Table 3 HIV-1 inhibition of the series **I** copolymers

Copolymer		The side-groups combinations in polymer (see Fig. 1) (% per the total **Z** capacity)					Anti-HIV effect	The HIV-1 strain
Sub-series	Sample	–y–$\mathbf{Z_0}$ = –**COCA**	–y–$\mathbf{Z_1}$ = –y–**SA**		–y–$\mathbf{Z_2}$ = –y–**Ali**		IC_{50}^{-1}, μM^{-1}	[a]
Ia $^{0}{}_{n=40}$	**1**	(100)	–	(0)	–	(0)	0.50	**EVK** [P]
							1.12	**Z** [P]
Ia $^{0+2}$	**2**	(92)	–	(0)	–$(CH_2)_2$–**CP**	(7.5)	0.60	**EVK** [P]
	3	(92)	–	(0)	–$(CH_2)_2$–**CH**	(7.5)	$\geq$0.29	**EVK** [P]
	4	(93)	–	(0)	–$CH(CH_3)$–**NB**	(7.7)	7.86	**IIIB** [D]
	5	(92)	–	(0)	–CH_2–$\mathbf{NB^{=}}$ *exo*	(7.8)	5.12	**EVK** [P]
							9.65	**Z** [P]
	6	(92)	–	(0)	–CH_2–$\mathbf{NB^{=}}$ *endo*	(7.8)	5.07	**EVK** [P]
	7	(92)	–	(0)	–CH_2–$\mathbf{NB^{O}}$	(7.7)	$\geq$3.84	**EVK** [P]
	8	(92)	–	(0)	–**AD**	(7.9)	5.75	**EVK** [P]
	9	(96)	–	(0)	–CH_2–**AD**	5.6)	5.26	**EVK** [P]
							10.30	**Z** [P]
	10	(94)	–	(0)	–$(CH_2)_2$–**AD**	(6.5)	4.70	**EVK** [P]
	11	(93)	–	(0)	–$(CH_2)_2$–NH–**AD**	(6.5)	3.63	**EVK** [P]
	12	(94)	–	(0)	–$(CH_2)_3$–**AD**	(5.4)	3.27	**EVK** [P]
							1.70	**899** [B]
	13	(93)	–	(0)	–CH_2–**DNB**	(7.5)	6.11	**EVK** [P]
							12.19	**Z** [P]
Ia $^{0+1}$	**14**	(60)	–C_6H_4–$\mathbf{SO_3^-}$	(40)	–	(0)	1.90	**Z** [P]
	15–18	(97 → 75)	–$(CH_2)_2$–$\mathbf{SO_3^-}$	(3 → 25)	–	(0)	0.18 → 2.62	**899** [B]
Ia $^{0+1+2}$	**19–23**	(89 → 67)	–$(CH_2)_2$–$\mathbf{SO_3^-}$	(3 → 25)	–CH_2–**NB**	(7.7)	0.16 → 0.87	**Z** [P]
	24–27	(89 → 67)	–$(CH_2)_2$–$\mathbf{SO_3^-}$	(3 → 25)	–CH_2–$\mathbf{NB^{=}}$ *exo*	(7.8)	0.16 → 0.78	**Z** [P]
	28–31	(90 → 68)	–$(CH_2)_2$–$\mathbf{SO_3^-}$	(3 → 25)	–CH_2–**AD**	(7.5)	0.56 → 0.20	**Z** [P]
Ib $^{0}{}_{n=30}$	**32**	(100)	–	(0)	–	(0)	3.01	**EVK** [P]
Ib $^{0+2}$	**33**	(95)	–	(0)	–CH_2–**AD**	(5.0)	<1.70	**EVK** [P]
Small molecular analog								
rimantadine			$An^- {}^+H_3N$–$CH(CH_3)$–$\mathbf{AD}$[b]				<0.0022	**899** [B]

[a] The experiments were carried out in partnership with: [**P**]—Natalia G. Perminova, Igor V. Timofeyev, et al. at the VBC "Vector" (Koltsovo, Novosibirsk Region, Russia); [**B**]—Marina E. Bourshtein in the laboratory of Prof. Alice G. Boukrinskaya at the Ivanovski Institute of Virology (Moscow, Russia), and [**D**]—Prof. Eric De Clercq, Rega Institute (Leuven, Belgium)

[b] Rimantadine is a well-known **AD**-type antiviral drug

$$\underset{\textit{docking energy minimum}}{\longleftarrow} \quad \mathbf{DNB} > \mathbf{AD} \sim \mathbf{NB}, \mathbf{NB^{\parallel}}, \mathbf{NB^{O}} >> \mathbf{CH}, \mathbf{CP} \quad \underset{\textit{antiviral efficiency}}{\longleftarrow} \tag{3}$$

The observed correlation supported identification of $(\mathbf{NHR})_3$ as the most probable target for the copolymers **I** during anti-HIV-1 activity. The maximum anti-HIV efficiency correlated with the maximal binding energy of the alicyclic anchors to the $(\mathbf{NHR})_3$. From a practical drug design point of view, the cage-type compounds (bi-, tri-, and tetra-cycles of norbornane (**NB/DND**) or adamantane (**AD**) derivatives (hydrophobic spheroids)) were found to be the most power anchors among the modelled side groups. Monocyclic cyclopentane (**CP**) and cyclohexane (**CH**) were qualified as energetically poor candidates inappropriate for the amplification of antiviral activity of the considered polymer macromolecules (Tables 3, 4). These correlations were notably useful examples of the applicability of docking to understanding and interpreting molecular mechanisms of bio-functionality of artificial molecules. However, beside the side groups (anchors) specificity, the polymer chain integrative role in the cooperative (synergistic) binding to the (nano) target required special consideration.

Polymer—cooperative effects

It is important to understanding why adamantane (**AD**) anchors do not provide significant anti-HIV activity in a small molecular state (Table 3, *rimantadine* control, see also the references [71, 72] for other AD containing

Table 4 Comparison of the in vitro and in silico data*

In vitro**:				**In silico:**						
Sample		Anti-HIV-1 effect $ln(IC_{50})$, mol/L		Model	Binding energy minimum, kcal/mol, scored under the docking via different score–functions:					
		"EVK"	**"Z"**	CH_3-**M1**	Dock6	PMF	D-	G-	MM GB/SA-	Chem-
Ia^0	**1**	−13.12	−13,93	–	0	0	0	0	0	0
Ia $^{0+2}$	**2**	−13.30	–	CH_3–**CP**	−15.8	−2.0	−28.6	−64.4	−14.3	−13.7
	6	−15.44	−16.08	CH_3–**NB**^{II} endo	−19.0	−5.7	−35.5	−74.9	−15.0	−16.2
	5	−15.45	–	CH_3–**NB**^{II} exzo	−18.9	−4.3	−36.2	−74.4	−14.8	−16.4
	9	−15.48	−16.15	CH_3–**AD**	−22.5	−9.2	−44.0	−93.0	−18.6	−18.6
	13	−15.63	−16.32	CH_3–**DNB**	−25.9	−9.5	−46.6	−104.4	−20.6	−20.0
Correlation			for "**EVK**" strain:		0.822	0.863	0.840	0.811	0.764	0.815
			for "**Z**" strain:		0.987	0.943	0.988	0.983	0.985	0.995

* Among the samples with varied side groups $\mathbf{Z}_2$ = **Ali**, and other comparable parameters of the structures

** In this table, the two experimental HIV-1 strains, EVK and Z, are shown independently

Table 5 (**CHR**/modelled ligands) + $(\mathbf{NHR})_3$ binding energies comparison

Docked model	Orientation	E (kcal/mol)	MM kD	−E/MM kcal/(mol × kD)
CHR within the 38 amino acids part, shown on Fig. 3	axial	−23.2*	4.8	4.8
M2 = H–CONH–CH_2-**AD** anchor with bridge (Fig. 6)	–	−21.4	0.19	112.6
M5 = CH_3–**AU**–**FU**–H	–	−19.6	0.36	54.1
M6 = H–**FU**–**AU**–**FU**–**AU**–**FU**–**AU**–CH_3 (Fig. 7)	axial	−30.3	1.05	28.7
M7 = [**FU–AU**]$_4$ + 2 terminal **AD** anchors (Fig. 10C)	belting	−58.0	1.68	34.5
M7 = [**FU–AU**]$_5$ + 2 terminal **AD** anchors (Fig. 10D)	axial	−70.6	2.02	35.0

E—the binding energies, summarised here for several of above noted models. *—labeled value was obtained from an AutoDock4 score reported previously [64, 65]. MM—molecular mass; the E/MM values can be used as criteria of binding efficiency per mass unit

compounds), whereas the same anchors integrated in a polymer become highly effective for HIV entry inhibition (Table 3, samples **8–12**, and references [7, 13–18, 26, 68]). The docking results reported here could explain this phenomenon: the "*single* anchor—target" contact was not energetically stable enough at physiological temperatures. Moreover, the small size of the anchor mono-point binding could not simultaneously cover all other binding sites (pockets and cavities) on the nano-target (Fig. 4).

Grafting many anchors along a flexible polymeric chain (containing additional carboxylic sub-ligands) changes this situation cardinally. The polymer cooperative macro ligand is capable of forming a multi-point binding network. This integration leads to a mutual stabilisation of multiple and variable by chemical nature interactions with a target. Even unstable (point-nonoptimal) contacts can be involved in the binding energy accumulation through the entire polymeric chain. If the size and adaptability of this chain is adequate for the nano-size and geometry of the target, the possible cumulative binding energy and blocking effect may be maximised.

Arrangement of the sub-structural components (–**Z**,–**Y**–, –**FU**–) of copolymer **I** molecules on a platform of a suitable length chain (determined by ***n***, the polymerization degree) toward minimal competition but mutually coordinated targeting to the $(\mathbf{NHR})_3$ may result in many fold enhanced binding (compare, for instance, binding energies of the models in Table 5).

As an irrational design example the co-integration of **CA**, **SA** and **Ali** could be noted. An evident decrease in the anti-HIV efficiency of all **Ali-**containing copolymers when the polymeric chain was simultaneously modified by **SA** side groups (compare **Ia**$^{0+1}$ with **Ia**$^{0+1+2}$, Table 3) correlated with the docking results: competitive interference of the **SA** and **Ali** components for too closely located binding sites. Specifically, **SA** contact with Lys^{574} in the $(\mathbf{NHR})_3$ pocket interfered with simultaneous binding of the **Ali** anchors to hydrophobic sites in the same pocket.

A rational design thus relates to the one-type (ether acidic SA or the hydrophobic **Ali**) side-groups cooperation based on the hydrophilic–anionic–flexible chain. For example, see the **Ali**-anchors containing **Ia** $^{0+2}$ sub-series of polymer samples (Table 3). Such a polymer macromolecule tuning resulted in increased recognition and blockade of target. This principle could be demonstrated on the docking

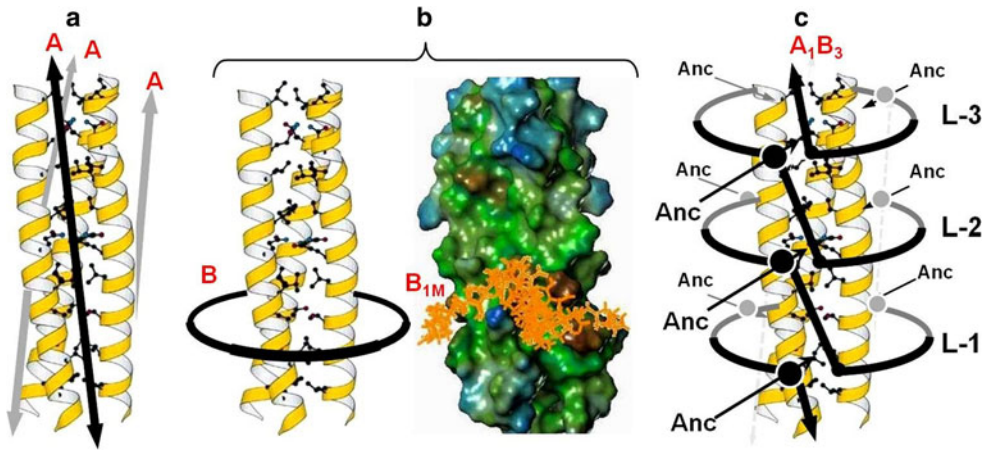

Fig. 11 The possible modes of polymeric chains orientation for blocking $(NHR)_3$ a Axial (**A**) orientation typical both for the viral fusion agents, the CHR, and for the M6 models (which can be extrapolated to the polymers Ia^0, Ia^{0+1}, and Ib^0; Fig. 7, Table 3). **b.** Belting (**B**) orientation discovered in models **M7** containing the effective **Ali**-type anchors **AD** or **DNB** (Fig. 10c). B_{1M} is an addition example of analogous docking of the models to the mutant $(NHR)_3$ target (PDB ID:1f23). The **M7** extrapolation corresponds to the samples Ia^{0+2} (Table 3). **c.** One of the possible variants of the combined orientation (A_1B_3), as an extrapolation corresponding to abilities of Ia^{0+2} copolymers, full-length chains of which are capable of anchoring (through anchors (**Anc**) = **Ali**) to the $(NHR)_3$ on all three **L1**-**L3** levels (nine pocket/cavity sites)

results reported here with an extrapolation to the synthetic chains. The ability of the polymeric **I** chains to interfere efficiently with the **CHR** (i.e., inhibit the HIV-1 fusion) is illustrated in Table 5. As indicated, the binding energy for a single **AD**-bridge **M2** model (related to *rimantadine*), as well as for the single co-monomer unit (**M5**), did not exceed the binding energy of the **CHR.** However, the binding power per unit molecular mass (-E/MM) for the **M2/M5** models was many times greater than the viral polypeptide. This is a good precondition for increased competitiveness via small ligand integrations in the rationally designed (polymeric) compounds, the molecular scale of which can be even smaller than the **CHR**. The binding energies of the **M6** and **M7** models confirmed this idea. The binding energy of the studied models estimated by docking correlated with the copolymers **I** having anti-HIV activity while the small molecule *rimantadine* was ineffective (Table 3).

The modelling and docking of the **Ia** chains displayed different possibilities for $(NHR)_3$ binding (Fig. 11). An axial (Fig. 11a) mode of binding to the target is used by the virus through the three **CHR** polypeptide regions of gp41 to initiate the HIV-1 fusion. The poly-carboxylic models **M6** (similar to the **CHR** as the negatively charged chains) possessed analogous ability to bind the target (Fig. 7). Thus, the docking forecasted considerable potency for the copolymers **I** (even without hydrophobic anchors) and the ability to competitively interfere with the **CHR,** preventing the virus fusion. This conclusion correlated with the appreciable HIV-1 inhibition observed for the polymer sub-series Ia^0 (sample **1**), Ia^{0+1} (samples **14-18**), and Ib^0 (also oriented axially) (Table 3).

The belting orientation (Fig. 11b) is theoretically more efficient for blocking **CHR** approach to $(NHR)_3$, and consequently a more effective inhibitor of the virus fusion. This mode of action was demonstrated above (Fig. 10c) to be typical for the flexible chain **Ia** copolymers containing effective **Ali** anchors every 3rd or 4th co-monomer unit. As seen from Table 3, attachment of **NB/AD/DNB**-type anchors to **Ia** flexible chains in a specific proportion strongly enhanced anti-HIV activity (sub-series Ia^{0+2}).[12] Conversely, an attempt to amplify the anti-HIV activity of the **Ib** chains by analogous insertion of appropriate anchors did not lead to a positive result. The Ib^{0+2} sub-series sample (Z_2 = **AD**) displayed 2 fold lower anti-HIV activity than did the anchor-free Ib^0 chain (Table 3). Therefore, selection of the optimal polymeric backbone is important in regulation of the molecular mechanisms of "synthetic—biological polymers" interactions. Backbone rigidity/flexibility, charged Z distribution, and other macromolecular parameters for drug design will be considered in forthcoming publications.

The bridge length is the next most important factor for switching the orientation of docked models from axial to belting (Figs. 9, 10). The docking results predicted more effective blockage of HIV-1 fusion by polymeric samples with short –Y– bridges. For example, within the Ia^{0+2} sub-series samples **8–12**, equipped with identical anchors (**Z** = **AD**) but different bridges, the following order for increased anti-HIV activity was observed (Table 3):

[12] With the exception of samples **2** and **3**, containing the inefficient anchors **CP** and **CH.**

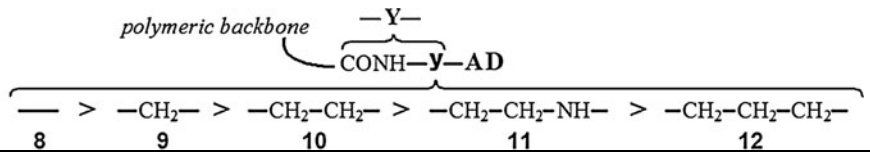

(4)

Along with the selection of chain, anchor, and bridge, the order of the anchor positioning within the chain is no less important for targeting. As defined via the docking of **M7** models, the distance between the anchors, most preferably in belting blockage, corresponded to grafting of the anchors at every 3rd or 4th co-monomer unit of the **Ia** polymeric chain. Every co-monomer unit has 4 positions for Z grafting (Fig. 1 or Table 3), and the 3–4 units have 12–16 positions. If we need only 1 anchor every 3–4 units, then (quantity of Z_2)/(quantity of $Z_2 + Z_0$) = 1/(12/16) = 0.06/0.08 (i.e., 6–8 %). This docking-predicted optimum correlated exactly with the modification degree (5–8 %) of the real samples selected from among the 170 candidates of series **I** as the most effective agents against HIV-1 in vitro (Table 3, **Ia** $^{0+2}$ sub-series). In practice, more rich content of the hydrophobic anchors in the co-polymers yielded no increase in anti-HIV efficiency, but did increase toxicity and decrease solubility in aqueous medium [26].

Step 3: extrapolation of the docking results to real-scale macromolecules

Subsequent extrapolation of the models M7 toward the **Ia** full-scale polymeric molecules led to the possibility of an artificial adjustment of their structure for a combined axial-co-belting binding to the $(\mathbf{NHR})_3$ target (Fig. 11, mode A_1B_3 as an example, or A_iB_j in the general case). An overall "programming" of the **Ia** molecules to the required HIV-1 fusion blocking includes (1) polymerisation degree $\boldsymbol{n}$ = 30–40 (for adequate size to bind $(\mathbf{NHR})_3$ with a A_iB_j mode); (2) the presence of effective (target pockets/cavities sensitive) anchors (**DNB** > **AD** > **NB**-type); (3) use of optimal (short) bridges to link the anchor to the polymeric backbone; and (4) optimal degree of chain modification with anchors (every 3rd or 4th co-monomer unit). Thus, the full-scale **Ia** polymeric chain modified with at least nine of the most efficient (**DNB**) anchors satisfied the requirements for $\mathbf{A_1B_3}$ binding capacity at the **L-1** to **L-3** levels of the $(\mathbf{NHR})_3$ target (Fig. 11, mode A_1B_3). Such a "programme" conforms specifically to the chemical structure parameters of the experimental sample **13** of the $\mathbf{Ia^{0+2}}$ sub-series, which possesses the maximal HIV-1 blocking activity (Table 3).

Conclusions and prospects for predictive drug design

Special attention should be paid to the fact that polymer-cooperative capacity cannot be achieved on a small molecule level. No small molecule can, in principle, be suitable for *macro*-molecular "programming" for full-scale interaction with a bio-polymeric target (as a rule, nano-object). This is why many attempts to develop a small-molecule inhibitor of the $(\mathbf{NHR})_3$ target led to only moderate inhibitors [55, 73], generally less effective than the active polymeric agents, represented in this study.

On the other hand, many small molecules, even weakly active ones, are very interesting sources for macromolecular design of novel, highly effective polymeric drugs, such as the **AD/NB/DNB** polymer-cooperated derivatives studied in this work. In view of this prospect, the modelling of synthetic—bio-polymer interactions becomes necessary. These interactions can be explored productively using the docking algorithm introduced in this article.

The most probable mechanisms of HIV-1 entry (fusion step) inhibition were investigated in this work. The knowledge obtained from applied docking methodology opened new doors to the design and development of antiviral drugs. Along with an HIV/AIDS prevention/therapy programme, the obtained data and molecular modelling strategy can be applied for the design of effective inhibitors of other (e.g., influenza) viruses utilising $(\mathbf{NHR})_3$-like fusion mediators of type 1 or 3 [74]. Particularly, it should be noted, that **AD**-containing compounds **8**–**12** of the **Ia** $^{0+2}$ series (Table 3) possessed inhibition activity against influenza viruses, including both rimantadin-sensitive and rimantadine-resistant strains [75].

The docking-confirmed principles of the polymer-cooperative multi-point blocking capacity explained why the novel polymeric agents prevented a drug resistance of viruses to these polymeric antivirals in contrast with small molecule prototypes [4, 21, 76]. For small molecules a single mutation only within one level (**L-1**) could be sufficient to avoid blocking of the targeted $(\mathbf{NHR})_3$ pockets. For comparison, HIV-1 $(\mathbf{NHR})_3$ resistance against polymeric multi-point blockers of the target (Fig. 11, AB_3) requires mutations at least on the three levels (**L-1**, **L-2**, and **L-3**). The probability of three-level mutations (occurring simultaneously within the viral target) is many times less than that of a single one-level mutation at **L-1**. This property apparently explains why the copolymer $\mathbf{Ia}^{0+2}$ sample **9** (Table 3) effectively prevented HIV-1 resistance in a long-term high-cycle experiment in spite of multiple mutative transformations [26]. Even within the one **L-1** level, an enhanced potency of the **M7** models was confirmed by docking on another $(\mathbf{NHR})_3$ target (PDB

ID:1f23) that had a I573T mutation within the binding pocket (Fig. 11b_{1M}, see also [24]). Taken together, these findings demonstrated the advantage of polymeric antiviral agents over small molecule antivirals in preventing drug resistance. This is promising aspect for a drug design development.

Acknowledgments The authors are thankful for the following collaborations: in copolymer synthesis, to Ekaterina Karaseva, et al. (Inst. Petrochem. Synthesis, Moscow); in anti-HIV-1 evaluations, to Marina Bourshtein, Alisa Bukrinskaya, et al. (Virology Inst., Moscow), Igor Timofeyev, Natalia Perminova, et al. (SRC "Vector", Koltsovo), Erik De Clercq, et al. (Rega Inst. Med. Res., Belgium); in support of the computational modelling, to Alexander Veselovsky, et al. (Inst. Biomed. Chem., Moscow); in provision of equipment and materials, to Olga Alikhanova; and in reviewing this paper and helpful discussion, to Lilia Alkhanova.

References

1. Huang SY, Zou X (2010) Advances and challenges in protein-ligand docking. Int J Mol Sci 11:3016–3034
2. Mohan V, Gibbs AC, Cummings MD, Jaeger EP, DesJarlais RL (2005) Docking: successes and challenges. Curr Pharm Des 11:323–333
3. Taylor RD, Jewsbury PJ, Essex JW (2002) A review of protein-small molecule docking methods. J Comput-Aided Mol Design 16:151–166
4. Index Nominum: International Drug Directory 20th Edition, MedPharm 2011, 2889 Pages, ISBN: 978-3-8047-5053-1
5. Maeda H (2012) Recollections of 45 years in research: from protein chemistry to polymeric drugs to the EPR effect in cancer therapy. ISBN: 978-1-61761-101-8
6. Kelly CG, Shattock RJ (2011) Specific microbicides in the prevention of HIV infection. J Int Med 270:509–519
7. Serbin AV, Karaseva EN, Tsvetkov VB, Alikhanova OL, Rodionov IL (2010) Hybrid Polymeric Systems for Nano-Selective Counter Intervention in Virus Life Cycle. Macromol Symp 296(1):466–477. http://onlinelibrary.wiley.com/doi/10.1002/masy.201051063/abstract
8. Rosenfeld R, Vajda S, DeLisi C (1995) Flexible docking and design. Annu Rev Biophys Biomol Struct 24:677–700
9. Dias R, de Azevedo Filgueira, Jr W (2008) Molecular docking algorithms. Curr Drug Targets 9:1040–1047
10. Nikolaienko TIu, Bulavin LA, Govorun DM (2011) The 5′-deoxyadenylic acid molecule conformational capacity: quantum-mechanical investigation using density functional theory (DFT). Ukr Biokhim Zh 83(4):16–28
11. Ponomar'ova AH, Iurenko IP, Zhurakivs'kyi RO, Hovorun DM (2011) Conformational capacity of 2′,3′-didehydro-2′,3′-dideoxyadenosine as a key to understanding its biological activity: results of quantum chemical modeling. Ukr Biokhim Zh 83(2):74–84
12. Bukrinskaya AG, Serbin AV, Bogdan OP, Stotskaya LL, Alimova IV et al (1993) Adamantane analogues block early steps of HIV infection. Antivir Res 20(1):63
13. Burstein ME, Serbin AV, Khakhulina TV, Alymova IV, Stotskaya LL et al (1999) Inhibition of HIV-1 replication by newly developed adamantane-containing polyanionic agents. Antivir Res 41(3):135–144
14. Serbin AV, Kasyan LI, Bourcteine ME, Boukrinskaya AG (1999) Norbornene containing antivirals: synthesis and evaluation of new polyanionic derivatives. Antivir Res 41(2):46
15. Timofeyev DI, Perminova NG, Kiseleva YaYu, Nekludov VV, Vatolin GYu, et al. (2003) HIV-inhibiting activity of polyanionic matrixes and based on them substances containing adamantane and norbornane pharmacophores. Antibiot Chemother (Russia) 48(5):7–15. http://www.ncbi.nlm.nih.gov/pubmed/12968467?ordinalpos=14&itool=EntrezSystem2.PEntrez.Pubmed.Pubmed_ResultsPanel.Pubmed_DefaultReportPanel.Pubmed_RVDocSum
16. Perminova NG, Serbin AV, Timofeev DI, Pliasunova OA, Karpyshev NN, et al. (2003) Experimental assesment of anti-HIV efficiency of complex membrannotropic substances including peptide pseudoligands. Biotechnology in Russia 5: 25–35. http://elibrary.ru/item.asp?id=8372899
17. Boukrinskaia AG, Serbin AV, Bogdan OP, Stotskaya LL, Alymova IV et al. (1996) Polymeric adamantane analogues. US Pat 5880154
18. Bukrinskaya AG, Burshtain ME, Alikhanova OL, Ermakov IV, Kasyan LI et al. (2006) Polyanionic derivatives of norbornane, method of synthesis and based on them inhibitors of human immunodeficiency virus reproduction. Rus Pat 2281297
19. Vorkunova GK, Kalinina LB, Burshtein ME, Serbin AV, Rodionov IL et al (2009) Effects of novel antiviral agents on HIV-1 replication. Vopr Virusol 54(2):27–31
20. Killian MS, Levy JA (2011) HIV/AIDS: 30 years of progress and future challenges. Eur J Immunol 41(12):3401–3411
21. Colman PM (2009) New antivirals and drug resistance. Annu Rev Biochem 78:95–118
22. HIV drug resistance, WHO information (2011) http://www.who.int/hiv/topics/drugresistance/en/index.html
23. Johnson VA, Calvez V, Gunthard HF, Paredes R, Pillay D et al (2011) Update of the drug resistance mutations in HIV-1. Top Antivir Med (IAS-USA) 19(4):156–164
24. Tsvetkov V, Veselovski A, Serbin A (2011) Polymer-Coupled Systems for Blocking the Viral Fusion 1. Modeling in silico the in vitro HIV-1 Entry Inhibitors. Antivir Res 90(2):A46. http://www.sciencedirect.com/science/article/pii/S0166354211001276
25. Serbin A, Karaseva E, Alikhanova O, Tsvetkov V (2011) Polymer-cooperative approach to multi-blocking the viruses. Antivir Res 90(2):A76. http://www.sciencedirect.com/science/article/pii/S0166354211002166, http://discover-decouvrir.cisti-icist.nrc-cnrc.gc.ca/fra/articles/?id=17926321
26. Serbin AV (2005) Design of bio-selective polymeric systems possessing the combined antiviral activity. D. Sci. Dissertation. http://www.lib.ua-ru.net/diss/cont/147035.html
27. Lu M, Ji H, Shen S (1999) Subdomain folding and biological activity of the core structure from human immunodeficiency virus type 1 gp41: implications for viral membrane fusion. J Virol 73(5): 4433–4438
28. Lu M, Stoller MO, Wang S, Liu J, Fagan MB et al (2001) Structural and functional analysis of interhelical interactions in the human immunodeficiency virus type 1 gp41 envelope glycoprotein by alanine-scanning mutagenesis. J Virol 75(22): 11146–11156
29. Tan K, Liu JH, Wang JH, Shen S, Lu M (1997) Atomic structure of a thermostable subdomain of HIV-1 gp41. Proc Natl Acad Sci USA 94(11):12303–12308
30. Koshiba T, Chan DC (2003) The prefusogenic intermediate of HIV-1 gp41 contains exposed C-peptide regions. J Biol Chem 278(9):7573–7579
31. Eckhardt M (2010) Quantitative analysis of the early steps of virus host cell interaction of human immunodeficiency virus type 1 and hepatitis C virus. Dis. D Nat Sci. Heidelberg, Germany: Ruperto-Carola Univ. 143 p.; http://archiv.ub.uni-heidelberg.de/volltextserver/volltexte/2010/10683/pdf/Dissertation_Manon_Eckhardt_Duplex.pdf
32. Hertje M, Zhou M, Dietrich U (2010) Inhibition of HIV-1 entry: multiple keys to close the door. ChemMedChem 5:1825–1835

33. Cai L, Jiang S (2010) Development of peptide and small-molecule HIV-1 fusion inhibitors that target gp41. ChemMedChem 5(11):1813–1824
34. Serbin A, Karaseva E, Chernikova E, Dunaeva I, Krutko E, et al. (2010) Graft and RAFT Reactive Macro Reagents: 3. Bis-[co-poly-(divinyl ether-alt-maleic anhydride)]-trithiocarbonate. Macromol Symp 296(1):80–91. http://onlinelibrary.wiley.com/doi/10.1002/masy.201051013/abstract
35. Serbin AV, Karaseva EN, Dunaeva IV, Krut'ko EB, Talyzenkov YA, et al. (2011) Controlled free-radical copolymerization of maleic anhydride and divinyl ether in the presence of reversible addition-fragmentation chain-transfer agents. Polym Sci - Series B 53(3-4):116–124. http://link.springer.com/article/10.1134%2FS1560090411030079
36. Cowie JMG (1985) Radical initiated alternating copolymerization. In: Cowie JMG (ed) Alternating copolymers. Plenum Press, NY, Ch 2, pp 19–74
37. Freeman WJ (1982) 13C NMR studies of the structure of divinyl ether-maleic anhydride cyclic alternating copolymer: a biologically active agent. In: Carraher C (ed) Biological activities of polymers—ACS Symp Series—American Chem Soc, Washington 243–253
38. Kunitake T, Tsukino M (1979) Radical cyclopolymerization of divinyl ether and maleic anhydride. A 13C-NMR study of the polymer structure. J Polym Sci Chem Ed 17(3):877–888
39. Samuels RJ (1977) A quantative evaluation of the structure and properties of the methyl ester of divinyl ether–maleic anhydride 1:2 copolymer. Polymer 18(5):452–460
40. Gorshkova MY, Lebedeva TL, Stotskaya LL, Slonim IY (1996) The structure of divinyl ether-maleic anhydride copolymer by spectroscopic methods. Polym. Sci. Ser. A, 38(10):1094-1096. http://cat.inist.fr/?aModele=afficheN&cpsidt=3266627, http://www.sciencedirect.com/science/article/pii/S0166354209001879
41. Tripos Inc.: 1699 South Hanley Rd., St. Louis, MO 63144-2917, 2007
42. http://spdbv.vital-it.ch/
43. Powell DJM (1977) Math program 12: 241–254; Powell MJD (1964) An efficient method for finding the minimum of a function of several variables without calculating derivatives. Computer J 7:155–162
44. Clark M, Cramer RD III, Van Opdenbosch N (1989) J Comp Chem 10:982–1012
45. Stewart JJP (2007) Semiempirical molecular orbital methods. In: Lipkowitz KB, Boyd DB (eds) Reviews in computational chemistry. Wiley, NJ, USA. doi:10.1002/9780470125786.ch2
46. Stewart JJP (1998) "PM3". In: Schleyer PVR, Allinger NL, Clark T, Gasteiger J, Kollman PA et al (eds) Encyclopedia Computat Chem, vol V 3. Wiley, Chichester, pp 2080–2086
47. MOPAC®; http://openmopac.net/
48. VEGA ZZ; http://www.vegazz.net/
49. Gasteiger J, Marsili M (1978) A new model for calculating atomic charges in molecules. Tetrahedron Lett 19(34):3181–3184
50. http://dock.compbio.ucsf.edu/
51. Connolly M (1983) Solvent-accessible surfaces of proteins and nucleic acids. Science 221(4612):709–713
52. http://www.cgl.ucsf.edu/Overview/software.html#dms
53. http://dock.compbio.ucsf.edu/DOCK_6/dock6_manual.htm
54. Hawkins GD, Cramer CJ, Truhlar DG (1995) Pairwise solute descreening of solute charges from a dielectric medium. Chem Phys Lett 246:122–129
55. Jiang S, Lu H, Liu S, Zhao Q, He Y et al (2004) N-Substituted pyrrole derivatives as novel human immunodeficiency virus type 1 entry inhibitors that interfere with the gp41 Six-Helix bundle formation and block virus fusion. Antimicrob Ag Chemother 48(11):4349–4359
56. Liu K, Lu H, Hou L, Qi Z, Teixeira C et al (2008) Design, synthesis, and biological evaluation of N-carboxyphenylpyrrole derivatives as potent HIV fusion inhibitors targeting gp41. J Med Chem 51(24):7843–7854
57. Zhou G, Wu D, Snyder B, Ptak RG, Kaur H et al (2011) Development of indole compounds as small molecule fusion inhibitors targeting HIV-1 glycoprotein-41. J Med Chem 54(20):7220–7231
58. Welch BD, Francis JN, Redman JS, Paul S, Weinstock MT et al (2010) Design of a Potent D-peptide HIV-1 entry inhibitor with a strong barrier to resistance. J Virol 84(21):11235–11244
59. Sabin C, Corti D, Buzon V, Seaman MS, Hulsik DL et al. (2010) Crystal structure and size-dependent neutralization properties of HK20, a human monoclonal antibody binding to the highly conserved heptad repeat 1 of gp41. PLoS Pathogens 6(11):e1001195. http://www.plospathogens.org/article/info%3Adoi%2F10.1371%2Fjournal.ppat.1001195
60. Chan DC, Fass D, Berger JM, Kim PS (1997) Core structure of gp41 from the HIV envelope glycoprotein. Cell 89(2):263–273
61. Follis KE, Larson SJ, Lu M, Nunberg JH (2002) Genetic evidence that interhelical packing interactions in the gp41 core are critical for transition of the human immunodeficiency virus type 1 envelope glycoprotein to the fusion-active state. J Virol 76(14):7356–7362
62. Markosyan RM, Ma X, Lu M, Nunberg JH (2002) The mechanism of inhibition of HIV-1 Env-mediated cell–cell fusion by recombinant cores of gp41 ectodomain. Virology 302(1):174–184
63. Qadir MI, Malik SA (2010) Genetic variation in the HR region of the env gene of HIV: a perspective for resistance to HIV fusion inhibitors. AIDS Res Hum Retrovir 26(11):1–7
64. Ramirez CGG (2007) Desino, sintesis y estructura de dominios helicoidales influencia la introduccion de aminoacidos D. Tesis Doctoral–Universitat de Barcelona, 60 p http://digital.csic.es/bitstream/10261/23028/6/Granados_Carmen_6.pdf
65. Gaston F (2008) Développement d'inhibiteurs d'entrée du virus VIH-1//These Présentée pour obtenir le titre de Docteur de L'Universite de Provence Aix-Marseillei. 250 p.; http://tel.archives-ouvertes.fr/docs/00/41/76/74/PDF/These.pdf
66. Muegge IA, Martin YC (1999) General and fast scoring function for protein-ligand interactions: a simplified potential approach. J Med Chem 42(5):791–804
67. IaIu Kiseleva, Perminova NG, liasunova OA, Timofeev DI, Serbin AV et al (2005) Antiviral action of membranotropic compounds modified by adamantane and norbornene pharmacophores exerted on different HIV-1 strains. Mol Gen Mikrobiol Virusol 2:33–36
68. Serbin A, Karaseva E, Egorov Y, Dunaeva I, Pavlova M et al (2009) A macromolecular basis for microbicides dual protecting against HIV and cytomegalovirus infection. Antivir Res 82(2):A66
69. Serbin AV, Veselovskii AV, Tsvetkov VB (2012) In vitro and in silico investigation of interferonogenic analogues of nucleic acids, artificially programmed to block the initial stages of HIV infection of cells. Appl Biochem Microbiol 48(9):723–739. http://link.springer.com/article/10.1134%2FS0003683812090049
70. Eldridge MD, Murray CW, Auton TR, Paolini GV, Mee RP (1997) Empirical scoring functions: I. The development of a fast empirical scoring function to estimate the binding affinity of ligands in receptor complexes. J Comp Aided Mol Des 11(5):425–445
71. Kolocouris N, Foscolos GB, Kolocouris A, Marakos P, Pouli N et al (1994) Synthesis and antiviral activity evaluation of some aminoadamantane derivatives. J Med Chem 37:2896–2902
72. Kolocouris N, Kolocouris A, Foscolos GB, Fytas G, Neyta J et al (1996) Synthesis and antiviral activity evaluation of some aminoadamantane derivatives. 2. J Med Chem 39:3307–3318

73. Frey G, Rits-Volloch S, Zhang XQ, Schooley RT, Chen B et al (2006) Small molecules that bind the inner core of gp41 and inhibit HIV envelope-mediated fusion. Proc Natl Acad Sci USA 103(38):13938–13943
74. Palfreyman MT, Jorgensen EM (2009) In vivo analysis of membrane fusion. In: Encyclopedia Life Sci, Wiley, Chihester, pp 1–14
75. Kozeletskaia KN, Stotskaia LL, Serbin AV, Munshi K, Sominina AA, Kiselev OI (2003) Structure and antiviral activity of adamantane-containing polymer preparation. Vopr Virusol (Russia) 48(5):19-26; PMID: 14598476. http://www.ncbi.nlm.nih.gov/pubmed/14598476
76. Lobritz MA, Ratcliff AN, Arts EJ (2010) HIV-1 entry, inhibitors, and resistance. Viruses 2:1069–1105